Rockfall Reconnaissance and Stability Assessment: Frenchman Coulee, WA

Ethan Guzek

A report prepared in partial fulfillment of

the requirements for the degree of

Master of Science
Earth and Space Sciences: Applied Geosciences

University of Washington

March, 2019

Internship coordinator:
Kathy Troost

Project mentor:
William C.B. Gates, McMillen Jacobs Associates

Reading committee:
Juliet Crider
Kathy Troost

MESSAGe Technical Report Number: 071

Executive Summary

The Sunshine Wall, a 30-meter tall outcrop of Columbia River Flood Basalt, is a popular climbing wall within Frenchman Coulee, located in central Washington. This study investigates the stability of the columnar basalt that makes up the wall, to educate climbers on how this slope fails and provide qualitative estimates of how close portions of the wall are to failure. Because the wall predominantly consists of columnar basalt, the most probable mode of large-scale slope failure is toppling. Some portions of the wall are "entablature," a highly fractured basalt which presents a significant risk with regard to rockfall. The stability of the Sunshine Wall was assessed using geomechanical rock mass classification systems, geometric measurements, and kinematic analyses. Data were collected using traditional field methods along with digital photogrammetry, from which I produced a high-density 3D point cloud and digital model of the wall. By combining traditional field methods and modern technology, a thorough and organized investigation was conducted. Data obtained by implementing these methods includes rock strength, rock mass ratings (quality), and kinematic analyses, which indicate that the columns are most likely to fail in direct toppling. Further, a simple qualitative center-of-mass analysis was applied to determine how close these columns may be to failure. Although many of the columns are stable, some are precariously balanced and may be unstable. In summary, the high strength of the intact rock, rough fracture surfaces, and lack of steeply dipping daylighting joints add to the stability of the slope. Low quality rock zones, areas with high densities of randomly oriented fractures, and the presence of potentially weak underlying material add to the instability of the slope. Climbers should use caution while belaying under zones of entablature, which are delineated in this study. They should also be aware of the conditions that lead to elevated risks of toppling failure. These conditions include columns that lean significantly away from the slope creating a large gap at the top of the colonnade, columns that are narrow and tall, and the presence of lower quality rock coinciding with the point at which a column might rotate away from the slope. To monitor the toppling hazard, the movement of key columns could be evaluated by repeatedly measuring the gaps at the top of the colonnade over time. These measurements will help to evaluate the significance of this hazard and whether or not these failures are slow and continuous or unpredictable and sporadic.

Acknowledgments

This project would not have been made possible without the funding provided by the American Alpine Club. I would like to extend a thank you to all those involved at the AAC for creating research opportunities such as this for myself and others. Individuals who provided critical guidance in the completion of this project include William C.B. Gates with McMillen Jacobs Associates, as well as Juliet Crider and Kathy Troost with the Department of Earth and Space Sciences at the University of Washington. I would like to thank my friends and classmates who visited the field with me and assisted in data collection. This group includes Martin Kanning, Chelsea Bush, Maddie Hille, and Hannah Karlsson. I would like to thank Jim Yoder and Marlene Ford for providing information on the history of rockfall and climbing at Frenchman Coulee. I would also like to thank the Wilbert R. Danner Fund for its contributions toward my education. Lastly I would like to thank my family for their unwavering support.

Table of Contents

List of Figures

List of Tables

Purpose and Scope

A history of rockfall and column collapse at the Frenchman Coulee Climbing Area inspired this study (Figure 1). Located east of the Cascade Mountains, the climbing area is used year round, but is especially busy in the spring and fall, with the crag experiencing hundreds of climbers on weekends (Mountaineers, 2018). Minor rockfall at climbing areas is a typical hazard and is anticipated by experienced climbers. Something that is often overlooked by recreational climbers, or even those with experience, is the possibility of large-scale slope failures, including column collapse and large block detachment. These types of failures occur less frequently and details of how these failures occur is less understood by the climbing community. On the other hand, rockfall and slope stability have been closely examined elsewhere by engineering geologists and geotechnical engineers over the last century (Turner, 2012). I apply traditional methods, used for the assessment of slopes with regard to protecting infrastructure, to the most popular wall of the climbing area, "The Sunshine Wall". In addition to these widely accepted and well documented methods, modern applications such as Structure-from-Motion (SfM) were implemented to create 3D models of the slope with sub-cm accuracy. These 3D point clouds allowed for a more objective examination of certain geometric measurements and for the detailed examination of inaccessible areas. By combining these methods, I was able to identify the dominant modes of failure of the slope as well as the key features that are indicative of slope instability.

Study Area

Geologic Setting

The predominant bedrock geologic unit in this area is the Columbia River Basalt Group which covers 200,000 square-kilometers of the Pacific Northwest, (Camp et al., 2003). Over 300 eruptive events occurred between 17.5 and 6 million years ago, during which massive amounts of flood basalt flowed from fissures located in Eastern Washington, Eastern Oregon and Western Idaho (Swanson et al., 1979a). Individual flows can reach thicknesses of 50 meters, and collectively these flows measure between 4-5 kilometers thick (Riedel et al., 2003). The Roza Member of the Wanapum Basalt, which can exceed 30 meters in thickness, tops the ridges near Vantage WA and was deposited between 15.3 and 14.5 million years ago (Reidel et al., 2003). Sourced from a 160 km long zone of fissures in Eastern Washington and Northeastern Oregon, the Roza Member is made up of four cooling units (Swanson et al., 1975). The Sunshine Wall is just one outcrop of a single flow of the Roza Member (Figure 2). The Squaw Creek Diatomite underlies the Roza Member. This siltstone unit measures 2-3 meters thick in most areas east of the Yakima River (Mackin, 1961). When hot lava flows over and interacts with sedimentary units peperite can form, which is a breccia of disintegrating basalt and sediment resulting from the explosive interaction between hot lava and wet sediment (Schmincke, 1967a). Approximately 2 km east of The Sunshine Wall, peperite in the Roza Member is well exposed in a road-cut (Reidel et al., 2003).

Within a given basalt flow, two facies can be distinguished based on the type of internal jointing (Figure 3). Entablature is characterized by closely spaced and randomly oriented joints. This is due to rapid cooling at the outer surfaces of the flow (Reidel et al., 2003). The colonnade, consisting of columns, is generally located beneath the entablature and has widely spaced joints that are often oriented vertically. In the Roza Member, the colonnade typically makes up ½ - ¾ of the thickness of the flow (Mackin, 1961). During the slow cooling process that forms the large columns, solidification fronts move inward from the top and bottom of the flow (Goehring and Morris, 2008). These cooling fronts originate from the upper and lower bounds of the flow, which are in contact with the cool air and ground upon deposition. The block size is larger in the colonnade due to the wider spacing of joints. Across The Sunshine Wall, columns are 1.7 meters wide and 22 meters tall on average, although some are as tall as 30 meters. At some locations the columns split into multiple smaller columns at the top of the colonnade. Due to the differences in the jointing between the entablature and colonnade, these two facies have different dominant modes of failure.

The Roza Member has a distinctive wavy appearance due to undulating vertical joints in the colonnade (Figures 2 and 3). Because the hexagonal columns are bounded by undulating joints they appear somewhat like crinkle-cut french fries, as opposed to perfectly planar-bound prisms. To describe the undulating surfaces, a kink angle can be assigned to measure the angle between adjacent faces. While a perfectly planar prism would have a kink angle of 180 degrees, past studies have found that joints in the Roza member can have a kink angle of 160 degrees. It is speculated that this phenomenon is created by oscillatory instabilities brought on when the joints become widely spaced (Goehring and Morris, 2008). Another interesting feature of the Roza Member is the presence of platy zones and vesicle sheets, which can be up to 1 and 3 meters thick, respectively (Thordarson and Self, 1998). Across The Sunshine Wall, the platy zones which are characterized by closely spaced sub-horizontal joints, are more easily weathered than the rest of the colonnade (Mackin, 1961). Both of these features can be laterally extensive in the Roza member, although no vesicle sheets were observed across The Sunshine Wall during this investigation, at least above the ground surface.

Tectonic Setting

The Sunshine Wall is located in a region with active faults and a history of at least one large earthquake. The closest fault to the Sunshine Wall is the Frenchman Hills Fault, which is located approximately 2.5 km to the south and is 120 km long. The active fault dips at 20-60 degrees to the northeast and movement is less than 0.2 mm per year (USGS, 2016). The largest tectonic event on record in eastern Washington occurred in December 1872 and is estimated to have had a magnitude between 6.5 and 7.0 (Brocher et al., 2017). The epicenter was located near Entiat, Washington which is approximately 80 km north of Frenchman Coulee. There are also a number of faults to the south of Frenchman Coulee that are capable of producing earthquakes with magnitudes above 7.0 (USGS, 2014).

Ice Age Flooding

The Columbia River Gorge, part of the Channeled Scablands of central Washington, was subjected to as many as 100 ice-age-floods between 20,000 and 14,000 years ago (Bretz, 1923a; USGS 2006). These floods had extensive erosive power, with flow velocities as high as 80 miles

per hour (Bjornstad, 2008), carving large waterfalls and wide gorges (coulees) through the Columbia River Basalts. The Frenchman Coulee served as one of several outlets during flooding. The alcoves within the coulee were created by headward erosion as the Wanapum Basalt was undercut (Reidel et al., 2003). Since then, the surrounding ridgelines have continued to fail creating talus slopes beneath the vertical walls (Figure 3).

Climate

The present climate in Central Washington is very dry, with the study area receiving an average annual 7.78 inches of precipitation (WRCC, 2016). In the summer, average monthly temperatures reach as high as 88 degrees F and in the winter they can drop to 19 degrees F (WRCC, 2016). In the winter, daily temperatures cycle above and below freezing. When it does rain, daily freeze-thaw cycles may accelerate the weathering of slopes via ice-wedging.

History of Climbing at Frenchman Coulee

Climbing at Frenchman Coulee began in 1948, although climbers did not venture over to the Sunshine Wall until the 1960's (Ford and Yoder, 2008). Of the different areas that form the crag today, the Sunshine Wall receives the most traffic. The portion of wall examined in this investigation measures approximately 400 meters across and 30 meters high, with the slope face dipping 90° ±10° and striking approximately 100°. Approximately 170 climbing routes exist across the colonnade on The Sunshine Wall (Ford and Yoder, 2008). Some routes use bolted anchors and some are climbed using traditional methods.

The talus slopes below the wall, along with the large boulders that rest at the base of the colonnade are direct evidence of how this slope has failed in the past (Figure 4). This is due to the toppling of precariously balanced columns. Climbers who are in possession of old guidebooks may find themselves looking for routes along the Sunshine Wall that no longer exist. One example of this, is the once precariously balanced column called "Herm's Tower" that was pushed over by unknown climbers in 2002 (Ford and Yoder, 2008).

During the course of this investigation a significant rockfall event took place. In late November 2018, freeze-thaw processes likely lead to ~33 cubic meters of rock detaching from the slope face and landing on the climbers trail below (Figure 5 and Appendix A). Approximately 33 meters of trail was covered by boulders and cobbles with freshly broken surfaces. Small craters measuring 70 cm in diameter, and 20-30 cm deep, were found on the trail. A sage tree that had taken root at the base of the slope was destroyed. Although few routes exist in the area where the rockfall occurred, the trail experiences large volumes of foot traffic to access the western half of The Sunshine Wall. Fortunately, during November the area is less busy and no one was hurt during this rockfall event.

Methods

The stability of the Sunshine Wall was assessed using geomechanical rock mass classification systems, geometric measurements, and kinematic analyses. Data were collected using traditional field methods (direct observation, distance measurements with tape measure and attitude measurements with a geologic transit compass). Additionally, digital photographs were collected

with a remotely-controlled quadrocopter (unmanned aerial vehicle, a.k.a. UAV or drone), from which I produced a high-density 3D point cloud and digital model of the wall.

The geomechanical rock mass classification took into account intact rock strength, rock quality designations (RQD) using Palmstrom's Volumetric Method, discontinuity conditions, discontinuity spacing, along with the orientations of joints and fractures relative to the rock slope (Bieniawski, 1989). Rock mass ratings (RMRs) were estimated at specific locations across the outcrop, following the protocol of Bieniawski, 1989. Fracture density and weathered state of the rock were examined across sections of highly resistant rock and compared to that of the platy zones which had a higher density of sub-horizontal joints and a higher degree of weathering. A standard Brunton compass was used to directly measure discontinuity orientations. Intact rock strength was estimated using a rock hammer (ISRM, 1978). I climbed the most popular routes across the Sunshine Wall to ensure that data was sampled from the entire height of the colonnade. In some locations apparent dip direction and dip measurements were estimated along fracture lines since some discontinuities, although persistent, did not create exposed planes.

To characterize the column separations, I measured the joint aperture at the base and top of the colonnade with a tape measure. Along the base almost all of the column separations were measured laterally. Walking across the top of the colonnade, separations could be measured laterally and in the dip direction of the slope face since I was looking down on the top of the columns. This information was used to characterize the magnitude and direction of displacement from original position on the rock slope, which assisted in identifying the dominant mode of failure.

Peak friction angle, which is required for a kinematic analysis, was determined by conducting a series of simple tilt tests (Kilche, 1999). Nearly planar pieces of talus found on the slope were stacked and slowly tilted until the top piece of talus began to slide. Once the top piece began to slide, the bottom piece of talus was held in place and the inclination of that surface was measured. Ten different combinations of talus pieces were used, with two tests per combination, to ensure that results were reproducible to within 5 degrees.

Kinematic analyses were carried out using a computer program called RocScience Dips to determine the likelihood of four major types of slope failure including slide, wedge, direct topple, and flexural topple (v7.013, 2018). Slope dip and dip direction, discontinuity orientations, and friction angle were the key inputs used in the analyses. The lateral limit, with respect to slope orientation, was set to 40 degrees since the strike of the slope varied by 20 degrees across the wall. This was done to account for oblique-directional failure orientations. Direct toppling failure was assessed by identifying at least two joint sets that intersected to form discrete blocks, in addition to a third joint set that acts as a release plane (Hudson and Harrison, 1997). The potential for sliding failure was assessed by measuring the inclination of column-cutting discontinuities and comparing that to the angle of friction (Wyllie and Mah, 2004). The potential for flexural toppling was assessed by searching for the presence of back-facing scarps associated with a series of layers dipping steeply into the slope (Wyllie and Mah, 2004). Wedge failure was investigated by searching for scenarios where two planes, oriented obliquely to the slope face, intersect to form a line that plunges out of the slope at an angle greater than the angle of friction (Wyllie and Mah, 2004).

To supplement data collected directly in the field, discontinuity orientations and lengths were also quantified using three-dimensional point clouds created using Structure-from-Motion (SfM)

photogrammetry. Images were obtained using a DJI Phantom 3 Pro remote-control helicopter, which was equipped with a 12.4-megapixel camera and consumer grade GPS unit. The focal length and sensor dimensions of the camera measure 3.6 mm and 6.317 x 4.738 mm respectively. Sub-cm ground sampling distances were achieved by flying within twenty meters of the wall. Flight paths were oriented vertically along the columns and pictures were taken with 70% minimum overlap. A total of 618 pictures were taken to construct the primary 3D model. When surveying under sunny conditions, sections of the Sunshine Wall were surveyed at specific times of day in attempt to keep the direction and amount of sunlight on the wall constant. Shutter speed and camera aperture were also changed manually throughout the flights to keep the level of exposure consistent between the images.

Pix4D (software v.4.2.27) was used to process the images to obtain a 3D model using default settings. The final 3D point cloud had an average ground sampling distance (GSD) of 0.75 cm. The global accuracy of the model had a horizontal uncertainty of approximately 5 meters. No significant distortion was noted in the model and a large portion of the Sunshine Wall was captured. More specifically, the Sunshine Wall was imaged between the "Tilted Pillars" area and a route called "Ride em Cowboy". The point density across the column faces was more than sufficient for the purpose of selecting points for plane fitting. The point cloud was used to measure heights and widths of columns, and allowed for specific observations to be documented in the WGS 84 / UTM Zone 11N (egm96) coordinate system. Additional ground control points were not surveyed with high grade GPS units in the construction of the model, as sub-cm global positioning is not essential for a stability analysis of this nature.

Accurately taking dip and dip measurements on column faces in the field proved to be difficult due to the irregularity of the surface shape and large kink angles. The waviness of the columns made it difficult to accurately measure the dip of the faces to within 10 degrees. The presence of magnetite in the basalt also interfered with magnetic compass readings in certain areas. In response to this, the 3D point cloud was used to select 20-30 points per column face (Figure 6). I wrote a script in MATLAB (R2018b) that was used to fit planes to these points using a least-squares fitting algorithm (Appendix B). From the planes I extract an average dip and dip direction for the selected column faces. This method was also used to measure fracture surfaces cutting through columns when sufficient surface area was exposed.

In order to individually assess certain columns with regard to topple failure, I use a simple geometric method to evaluate whether the center of mass of the column projected vertically outside of the base of the column. This was done by comparing the ratio of the base width and column height directly to the tangent of the basal plane angle (Wyllie and Mah, 2004). Using this comparison in combination with the block-like geometry of the columns, the equation was further simplified to also compare the base widths with the size of column separations at the top of the colonnade (Figure 7). The derivation is given on Fig. 7 and uses the trigonometric identity associated with taking the sin of an inverse tangent, plus the assumption that the column height is significantly greater than the column base. This was done to see if simpler, more repeatable, measurements could be made to assess the factor of safety with regard to direct toppling. The assumptions required for the b/h-tan(Φ) comparison to be applicable to topple analysis were that the columns be uniform in shape for the entire height of the column, that the column is free-standing, and that a plane exists from which the column can detach. For the direct width-separation comparison it was also assumed that the column faces behind the column of interest

were dipping at 90 degrees. Factors of safety were directly calculated using the two end-type equations (boxes on Fig. 7) with field and digital measurements used for the critical variables.

Assuming the geometric conditions shown in Figure 7 were met, the measured parameters were back-calculated to produce indirect measurements of basal plane angle and column separation using the 2 end type equations. This was done to assess the validity of the proposed-simplified comparison.

Results

Intact Rock Mass

The basalt making up The Sunshine Wall consists predominantly of colonnade that exhibits variable strength and degrees of fracturing. Fresh surfaces of the Roza Member have a blue appearance. The majority of the exposed rock mass has been slightly weathered on the surface and is a deep reddish brown in direct sunlight. The majority of the colonnade is made up of good-very good rock and is massive in texture (Bieniawski, 1989). Results from geologic hammer tests indicate that the rock is medium strong to very strong, consistent with an estimated uniaxial compressive strength of 50-250 MPa. The RQD measurements calculated using the method from Palmstrom (2005) were between 50% and 80% for the high quality rock mass making up the column faces. These are attributes of a strong rock mass, as reflected in the RMR of 80-90 assigned to the majority of the colonnade. While RMR of the entablature was not assessed, fracture density was relatively higher, fracture orientations were more variable, and curving fracture surfaces were more common in the entablature than in the colonnade, suggesting a lower RMR.

Weathered Zones

Across the colonnade there were platy zones where lower quality rock was observed. The RQD calculated using the method from Palmstrom (2005) ranged between 10% and 30% for these platy zones, which showed a higher density of sub-horizontal joints specifically. Silty dust covered the fracture surfaces and loose rock could easily be plucked out using my fingers. These rock fragments were easily broken with a rock hammer, indicating that the strength of this rock was lower than that of the intact rock faces. At some platy zones the column width narrows, suggesting some rock has been removed by erosion (Figure 8). The RMR of the weathered zones, within the colonnade, was consistently close to 50. A number of the low RMR zones across the Sunshine Wall and adjacent Kotick Memorial Wall are all within a 5-meter vertical span in elevation. In oblique aerial photographs a prominent linear feature within this elevation band extends across a 140-meter stretch of the Sunshine Wall (Figure 9). This feature coincides with some of these low RMR zones and many of the tops of past-failed columns.

Discontinuities

The results from the discontinuity survey are summarized in Figures 10 and 11. Randomly striking vertical joints separate the hexagonal columns (Figure 11a). The joints generally have open to very wide aperture (0.25-10 cm) with no infilling, and are widely spaced (0.6-2 meters). The joints are persistent for 20-30 meters and are undulating with rough surfaces. The lower extent of the joints is not visible, while the visible end terminates at the top of the climbing wall.

There are also non-systematic discontinuities which are persistent across the widths of the columns and have very tight aperture. Many of these discontinuities are nearly horizontal, although the average dip is 18 degrees (Figure 11b). The surfaces are also very rough and irregular in shape which adds to the effective friction angle.

The angle of friction was determined based on the results of the 20 tilt tests conducted in the field. Upon the tilting of the stacked rocks, sliding began at an average angle of 41 degrees with a standard deviation of 2 degrees (Appendix D). The resulting slide angle from each combination of talus pieces was reproducible to within 0-5 degrees. This average sliding angle was used as the angle of friction in the kinematic analyses.

Column Separations

On average, the column separations are greater at the top of the colonnade than at the base by 20 cm, although in some areas they differed by as much as a meter (Figure 12). Along the top of the colonnade separations are generally greater toward the slope face (Figure 13a). Some column separations are greater than a meter at the top of the colonnade while the separations at the base are mostly less than 10 cm, indicating a significant amount of differential movement (Figure 13b; Table 1). At locations where separations at the top of the colonnade are large, column faces dip into the slope.

Kinematic Analysis

Kinematic analyses using the RocScience Program Dips 7.013 indicated that the slope is most likely to fail in direct topple (Figure 14a). This is due to the high number of vertical joints that form tall rectangular blocks, along with the presence of sub-horizontal joints and low RMR zones which act as release planes.

The other failure modes (slide, wedge, and flexural toppling) were assessed as well but did not demonstrate the same likelihood of failure (Figures 14b-d). This is due to a lack of intermediately dipping joints between sub-horizontal and vertical. Chances of slide failure are not as high because the dip of the majority of column-cutting fractures were well below the angle of friction, although there were several discontinuities that had dips measuring close to the angle of friction. A prominent discontinuity cuts across the column associated with the climbing route Steel Pulse at an angle of 38 degrees (upper surface highlighted in Figure 11a). Since the dip of this surface is just one degree less than the standard deviation of the mean friction angle, the factor of safety for sliding on this surface is close to one.

Wedge failure conditions were not observed to be likely, as the joints separating the columns were all grounded. No scenario was observed where an intersection line of two planes day-lighted into the slope face. Additionally, when columns were not randomly tilting into each other they were essentially free standing. The variability of column-face dip directions and irregularity of the slope direction does not lend itself to a situation where flexural toppling is applicable.

Topple Analysis

A factor of safety analysis was carried out for a number of columns that appeared to show significant differential separation between the top and base of the colonnade. Although assessments could not be conducted for every single column, individual topple assessments were conducted for the routes known as Sunshine Buttress, Midsummer Night's Dream, In Too Deep, Steel Pulse, Throbbing Gristle, Peaceful Warrior, and Anthropomorphic Chest of Drawers. These routes were chosen because they appeared to be especially at risk with regard to topple failure. This analysis was done to show example calculations and to present an idea of how close these columns may be to failure. A route known as Desert Dessert, which is outside the immediate study area, was included as well because it is well known and the column showed significant differential separation between base and top. Factors of safety were calculated using the traditional comparison presented in Wyllie and Mah (2004), as well as the direct width-separation comparison (Figure 7). Based on results from these wo comparisons, the factors of safety for the columns that were inspected range from 0.76 to 3.

A factor of safety plot was created for each comparison (Figure 15). Figure 15a shows the factor of safety in terms of the basal plane angle ($\tan\Phi$) and the base-height ratio, while Figure 15b compares the column width and separation directly. The traditional comparison consistently estimates columns to have a lower factor of safety than that estimated by the direct width-separation comparison. Results based on the traditional comparison indicate that three columns should have already failed.

In back-calculating certain parameters to compare the two methods for toppling analysis, I see significant inconsistencies for some columns. The difference in back-calculated values and measured values for column separation and column face dip angle are presented in Table 2. The average difference in the column separation and column face dip angle was 67 cm and 1.85 degrees respectively. For columns that are relatively more uniform in shape, such as Desert Dessert and the Anthropomorphic Chest of Drawers, the two methods are more agreeable. The afore-mentioned inconsistencies and columns exhibiting factors of safety below 1 are discussed below.

Discussion

Dominant Mode and Style of Failure

Evidence of direct toppling is supported by the kinematic analysis, which highlights the presence of column faces that dip steeply into the slope, in addition to field observations of significant column separations at the top of the colonnade. Of particular note are the differences in RMR between the platy zones and massive-intact rock mass, and the consistent elevation at which the tops of past-failed columns and these low RMR zones exist. The rock mass comprising the low RMR zones likely has a lower compressive strength, and thus could be vulnerable to bearing failure. This is when the rock breaks due to the weight of overlying rock. If weathering weakens rock in the low RMR zones, those zones may not be able to sustain the weight of the column above. These zones would then provide a surface from which the column could rotate outwards. It is my interpretation that slow-continuous column separation is being accommodated by bearing failures of low RMR zones in the middle and base of the colonnade. Although not

observed directly along The Sunshine Wall, peperite may underlie the Roza Member beneath the ground surface which would similarly lead to bearing failures.

These low RMR zones display higher degrees of weathering, higher fracture density, and significant erosion which effectively reduces the width of the column at that location. This reduction in column width reduces the stability of the column by decreasing the base-height ratio, and therefore allowing the center of mass to more easily fall outside the base-footprint of the column. Given the low quality of rock at these zones, it is plausible that bearing failures are occurring and rotation is being accommodated as rock material is crushed under the weight of the column, or as material is altered by weathering and removed by erosion.

Some columns that are overhanging significantly do not show a weathered zone above the ground surface. It is possible for a weathered zone to exist below the ground surface which would similarly explain the movement of the column. If this was the case the relevant column height would increase which would reduce the stability of the column (Figure 7). On the other hand, since the point at which the column is rotating would be below ground, there would also be some buttressing effect from the soil and rock at the base of the column. Buttressing effects are also present where columns contact each other near the middle and top of the colonnade. Forces associated with buttressing effects were not taken into account when conducting the topple analysis. This is important in understanding the limitations of the simple center-of-mass model being used in this study.

Differences in Topple Analysis Comparisons

The assumptions required for the b/h-tan(Φ) comparison to be valid were that the columns be uniform in shape for the entire height of the column, that the column is free-standing, and that a sub-horizontal plane exists from which the column can detach. For the direct width-separation comparison it was also assumed that the column faces behind the column of interest were dipping at 90 degrees, as theta is measured off vertical. The columns assessed followed or deviated this criterion to varying degrees.

Some columns have a considerably wavy shape making the width of the column vary across its height. The width used in modeling topple failures was chosen to represent the width of the column close to where rotation was occurring (Figure 8). Some columns also bend, narrow, or widen at the top of colonnade. This significantly changes the location of the column's center of mass compared to the center of mass for a uniform-rectangular prism.

Significant differences between measured values and back-calculations were noted. This is due to the geometry and conditions of real world situations not meeting the necessary criteria for the topple analysis to be entirely accurate. This reveals that these calculations may be more qualitative than quantitative for some columns. I believe one major reason why the direct width-separation comparison predicts consistently higher factors of safety, is that the dip of the adjacent column faces further into the slope are not accounted for. In order for the analysis criteria to be met, the dip of the adjacent column should be 90 degrees. If the second column into the slope face is also leaning forward, then the resulting column separation would be smaller and a higher factor of safety would be calculated.

An alternative explanation would be that the entire digital model is tilted to the south. Although no distortion or abnormalities were observed, slight tilting could have gone unnoticed. This would result in the dip of overhanging column faces being over-predicted by possibly 1 degree or less. This could account for a small portion of the difference between the two comparisons.

Case Studies

The column associated with Midsummer Night's Dream (Figure 16) was assessed qualitatively, since criteria for the standard topple analysis is not met. The column curves outward and thus the center-of- mass is shifted away from the slope in a manner not accounted for in the simple geometry of the standard toppling analysis. In fitting a plane to this curved column face, the apparent dip effectively increased by 1 degree, making the factor of safety lower. Accepting these deviations, the results indicated a pseudo-FS calculation below 1. Approximately 10 meters from the base of the column the width also appears to narrow, which further leads to instability (Figure 16).

During field investigations, the significant leaning of the column hosting the route Peaceful Warrior was not noticed. Analysis indicates that the factor of safety may be below 1, although it appears that buttressing effects are present at the base of the column. It also appears that there is significant contact between the north-dipping face and the adjacent column, making the column not entirely free standing. This contact creates friction which adds an element of stability to the column.

The column associated with Anthropomorphic Chest of Drawers is shown in the center of Figure 16. Results of the traditional comparison indicated a factor of safety below 1. An interesting aspect of this column is that no sub-horizontal joints were observed where the column rotates away from the slope. The column appears to curve abruptly at this location causing separation to increase towards the top (Figure 17). The lack of a release plane likely adds to the stability of this column.

Steel Pulse is one of the wider columns. The width of its base adds to its stability, despite its steeply overhanging faces. This column shows all the signs of instability that have been observed across the Sunshine Wall and is a good way to summarize the observations that help identify instability. First, the column dips at an angle between 85 and 86 degrees which is significant enough to cause instabilities for some columns. Secondly, a low RMR zone exists at the base of the column, consistent with the idea of bearing-failure facilitating column separation that could lead to toppling. Third, there is a steeply dipping discontinuity that invites the possibility of slide failure in addition to topple failure. For instance, if the column leans out further it could either topple, or the top half of the column could slide off, if the through-going plane is rotated forward significantly. Another item observed around this column was that there was larger than typical column separation behind the base of the column. This could be due to a bearing failure of the geology beneath the ground surface, whether that be peperite or a thick-low RMR zone that extends below the ground surface.

Applicability of the Topple Analysis

Despite the center of mass comparisons being only approximate for some situations, the topple analysis is still a very useful tool to monitor the stability of specific columns. Repeat SfM surveys could be conducted or simple column separation measurements could be carried out intermittently. An example location of a potential monitoring point is atop the routes Sunshine Buttress and Mix it Up (Figure 13b). In Too Deep is another route that could easily be monitored. It should be noted that columns split into multiple columns at some locations, and that it is important to compare the column separation with the base-width of the column (the point at which the column rotates away from the slope). Given the assumptions and approximations of this simple stability analysis, it is important to note that a column is not guaranteed safe to climb even if the separation is less than the width.

Although less likely, other modes of failure should not be forgotten. Not very many of the through-going discontinuities were oriented steeper than the angle of friction but some did exist and some may have been missed in the discontinuity survey.

Utility of SfM

The use of SfM allowed for the completion of stereonets which were used for kinematic analysis. It was also instrumental in documenting observations across the colonnade. Although instrumental in this investigation, SfM technology could not replace hands-on field work entirely. Many of the discontinuities cutting across the long axis of the columns did not have significant surface area exposed. Although the 3D model has sub-cm accuracy the area exposed would have to be at least 10 cm in all directions to obtain reasonably accurate measurements. There were few locations where this was the case. Low RMR zones would not have been able to be identified solely based of SfM results. By combining traditional geologic methods with SfM technology, a thorough and organized analysis was efficiently conducted.

In the future, implementing ground control GPS points would provide consistency between repeat surveys. These points would be best taken atop the columns or on the basin floor below to obtain good GPS signal and not have the wall block half of the horizon for satellite coverage.

Conclusions and Recommendations

The Sunshine Wall has had, and will continue to have, toppling failures in addition to significant rockfall sourced from zones of entablature. Causes of instability include the weathering of platy zones and underlying geology. Factors adding to the stability of the Sunshine Wall include buttressing effects as well as rough-irregular joint surfaces which add to the effective friction within the rock mass.

As columns are preferentially weathered along platy zones and beneath the ground surface, rotating and tilting of columns will continue until toppling occurs. Although this movement cannot be stopped, it can be monitored. Precise repeat measurements of column separations over time could easily be implemented to reveal which columns are currently moving. The frequency at which failures occur is not well constrained as people have been climbing here for a relatively short span of time. Even shorter is the length of time that the slope has been studied.

Measurements and calculations with regard to the factor of safety analysis presented in this study should be seen as qualitative and educational. I do not take any responsibility in stating that any route located within this climbing area is safe or unsafe. Climbers can take information presented in this study and decide for themselves whether they are willing to climb a given route. In general climbing is dangerous, and rockfall as well as topple failure are hazards and risks that should be accepted if participating in the activity. I hope that the information presented here helps climbers make safe decisions.

For climbers visiting the crag, attention should always be given to small scale rockfall. For example, caution should be used when spending time at the base of the Air Guitar Area. There are many popular routes at this location and belayers will be spending prolonged periods of time standing at the base. Similarly, caution should be used when crossing the trail where the November 2018 rockfall event occurred. With respect to topple failures, columns are more at risk if they lean significantly away from the slope, if they are narrow and tall, and if lower quality rock exists at a point where the column rotates away from the slope.

References

Bieniawski, Z.T., 1989, Engineering rock mass classifications: a complete manual for engineers and geologists in mining, civil, and petroleum engineering. New York, Wiley, 272 p.

Bjornstad, B., 2008, The Ice Age Floods through the Western Channeled Scablands: Northwest Geologic Society. Society Field Trips in Pacific Northwest Geology, 24 p.

Brocher, T.M., Blakely, R.J., and Sherrod B.L., 2017, Evaluating Spatial and Temporal Relations between an Earthquake Cluster near Entiat, Central Washington, and the Large December 1872 Entiat Earthquake: Bulletin of the Seismological Society of America, v. 107, no. 5, p. 2380-2393, doi:10.1785/0120170113.

Camp, V.E., Hanson, W.E., and Ross, M.E., 2003, Genesis of flood basalts and Basin and Range volcanic rocks from Steens Mountain to the Malheur River gorge, Oregon: Geological Society of America Bulletin, v. 115, p. 105–128.

Ford, M., Yoder, J., 2008, Frenchman Coulee: A Rock Climber's Guide, Eatonville, WA, HomePress Publishers.

Goehring, L., and Morris, S.W., 2008, The scaling of columnar joints in basalt: Journal of Geophysical Research, v. 113, doi:10.1029/2007JB005018.

Grolier, M.J., Bingham, J.W., 1978, Geology of Parts of Grant, Adams, and Franklin Counties, East-Central Washington: Department of Natural Resources Division of Geology and Earth Resources. Bulletin No. 71.

ISRM (International Society for Rock Mechanics), 1978, Suggested Methods for the Quantitative Description of Discontinuities in Rock Masses. International Journal of Rock Mechanics and Mining Sciences & Geomechanics Abstracts, v. 15, p. 319-36

Kilche, C.A., 1999, Rock Slope Stability. CO, Society for Mining, Metallurgy, and Exploration. p. 39.

Mackin, J.H., 1961, A stratigraphic Section In the Yakima Basalt And The Ellensburg Formation In South-Central Washington: Department of Conservation, Olympia, Washington. Divison of Mines and Geology. Report of Investigations No. 19.

Palmstrom, A., 2005, Measurements of and Correlations between Block Size and Rock Quality Designation (RQD): Tunnelling and Underground Space Technology, v. 20, no. 4, p. 362-377.

Pix4D (2018). Professional photogrammetry and drone-mapping. Version 4.2.27.

Reidel, S.P., Martin, B.S., and Petcovic, H.L., 2003, The Columbia River flood basalts and the Yakima fold Belt: Geologic Society of America Field Guide 4.

RocScience Inc. (2018). DIPS, Plotting and Analysis Software for Geomechanical Structural Data. Toronto, Version 7.013. Canada.

Schmincke, H-U., 1967a, Fused tuff and peperites in south-central Washington: Geological Society of America Bulletin, v. 78, p. 319–330.

Swanson, D.A., Wright, T.L., Hooper, P.R., and Bentley, R.D., 1979a, Revisions in stratigraphic nomenclature of the Columbia River Basalt Group: U.S. Geological Survey Bulletin 1457-G, 59 p.

Swanson, D.A., Wright, T.L., Heltz, R.T., 1975, Linear vent systems and estimated rates of magma production and eruption for the Yakima basalt on the Columbia Plateau: American Journal of Science v.275, p.877-905

The Mountaineers, 2018, SECOND VANTAGE TOILET OPEN FOR 'BUSINESS': https://www.mountaineers.org/blog/second-vantage-toilet-open-for-business (Accessed January 2019)

Thordarson, T., Self, S., 1998, The Roza Member, Columbia River Basalt Group: A gigantic pahoehoe lava flow field formed by endogenous processes: Journal of Geophysical Research Vol. 103, No. B11, p. 27,411-27,455.

Turner, A.K., Schuster, R.L., 2012, Rockfall Characterization and Control. Washington D.C, Transportation Research Board.

United States Geologic Survey, 2016, Frenchman Hills structures, Frenchman Hills fault (Class A) No. 561a: https://earthquake.usgs.gov/cfusion/qfault/show_report_AB_archive.cfm?fault_id=561&section_id=a (Accessed February 2019)

USGS, 2014, USGS Earthquake Scenario Map (BSSC 2014): http://usgs.maps.arcgis.com/apps/webappviewer/index.html?id=14d2f75c7c4f4619936dac0d14e1e468 (Accessed February 2019)

United States Geologic Survey, 2006, The Channeled Scablands of Eastern Washington: https://www.nps.gov/parkhistory/online_books/geology/publications/inf/72-2/contents.htm (Accessed February 2019)

Western Regional Climate Services, 2016, Quincy 1 S, Washington (456880): https://wrcc.dri.edu/cgi-bin/cliMAIN.pl?wa6880 (Accessed December 2018)

Wyllie, D.C., Mah, C.W., 2004, Rock Slope Engineering Civil and Mining 4th Edition Based on the third edition by E Hoek and J Bray: New York, Spon Press.

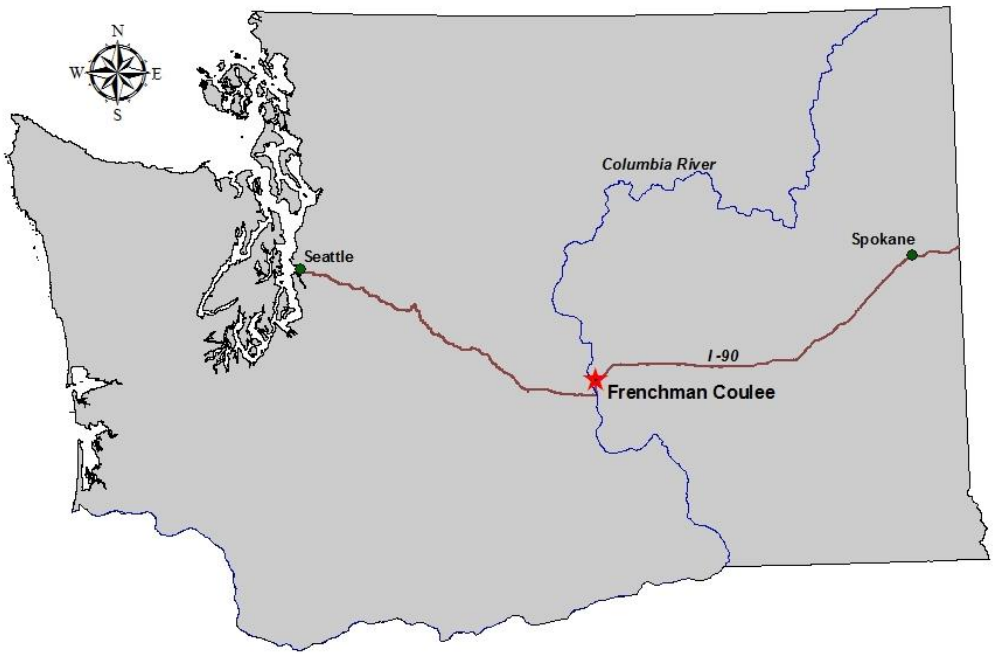

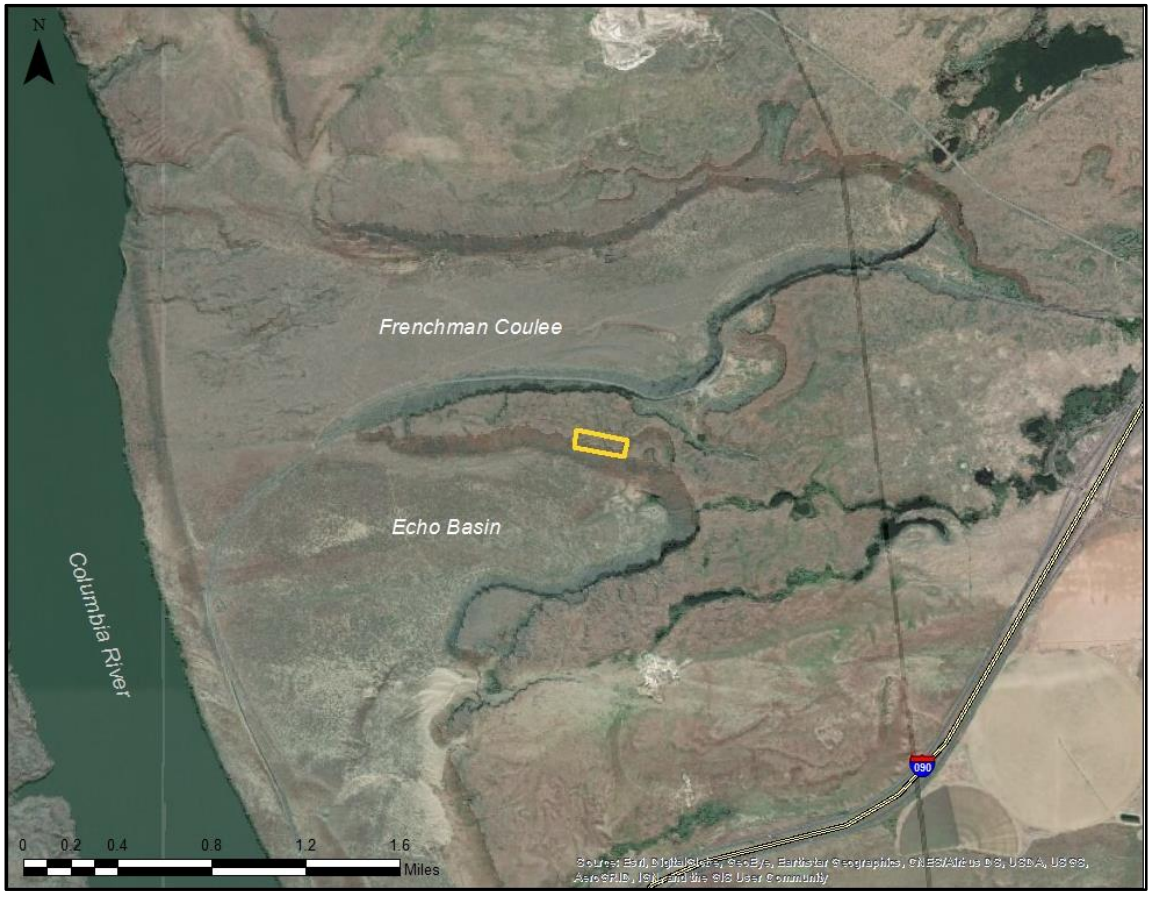

Figure 1: Study area location. Top: Location of Frenchman Coulee in Washington State. Bottom: Aerial image showing the environment surrounding the study area. The Sunshine Wall is outlined in yellow. Interstate 90 crosses the southwest corner of the image.

Figure 2: Site Overview. Top: Oblique aerial view of the site area from the south. The Sunshine Wall is located on the eastern side of the E-W trending ridge that separates Echo Basin and Frenchman Coulee. Image from Google Earth. Elevations are in terms of distance above mean sea level. Bottom: Sunshine Wall from the floor of Echo Basin. Location from which the photo was taken is shown on the image above; indicated by green dot.

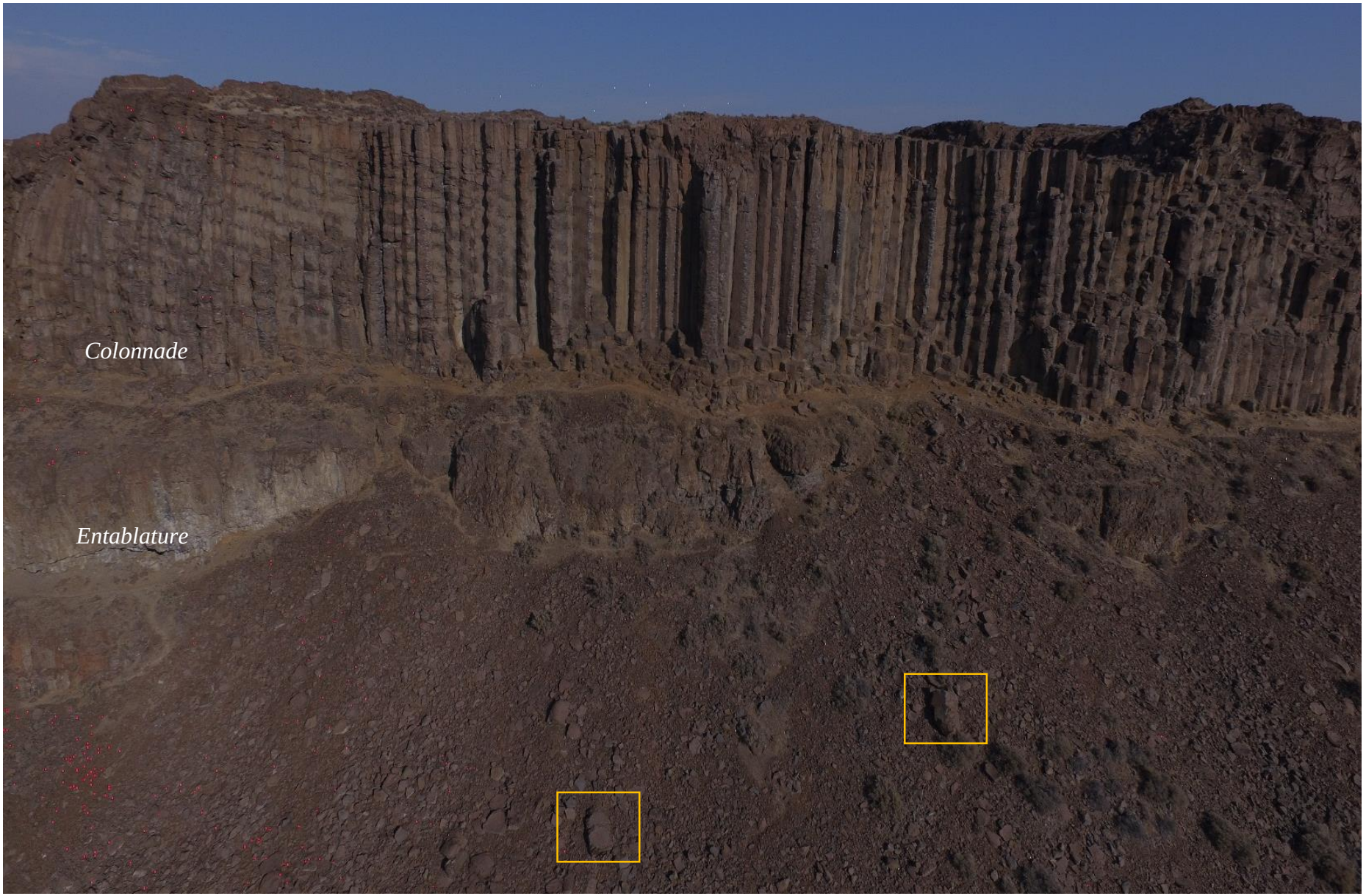

Figure 3: Oblique aerial image of the western extent of the Sunshine Wall. Camera is facing north. Basalt columns are approximately 1.7 meters wide and 22-30 meters tall. Below the colonnade, the entablature and the talus slope are shown. Note the presence of columnar shaped blocks on the talus slope (yellow boxes).

Figure 4: Column-sized debris at the base of the colonnade, Sunshine Wall. Image of the climbing trail at the western extent of the study area. Similar to the talus slope, large column sized blocks have accumulated at the base of the wall.

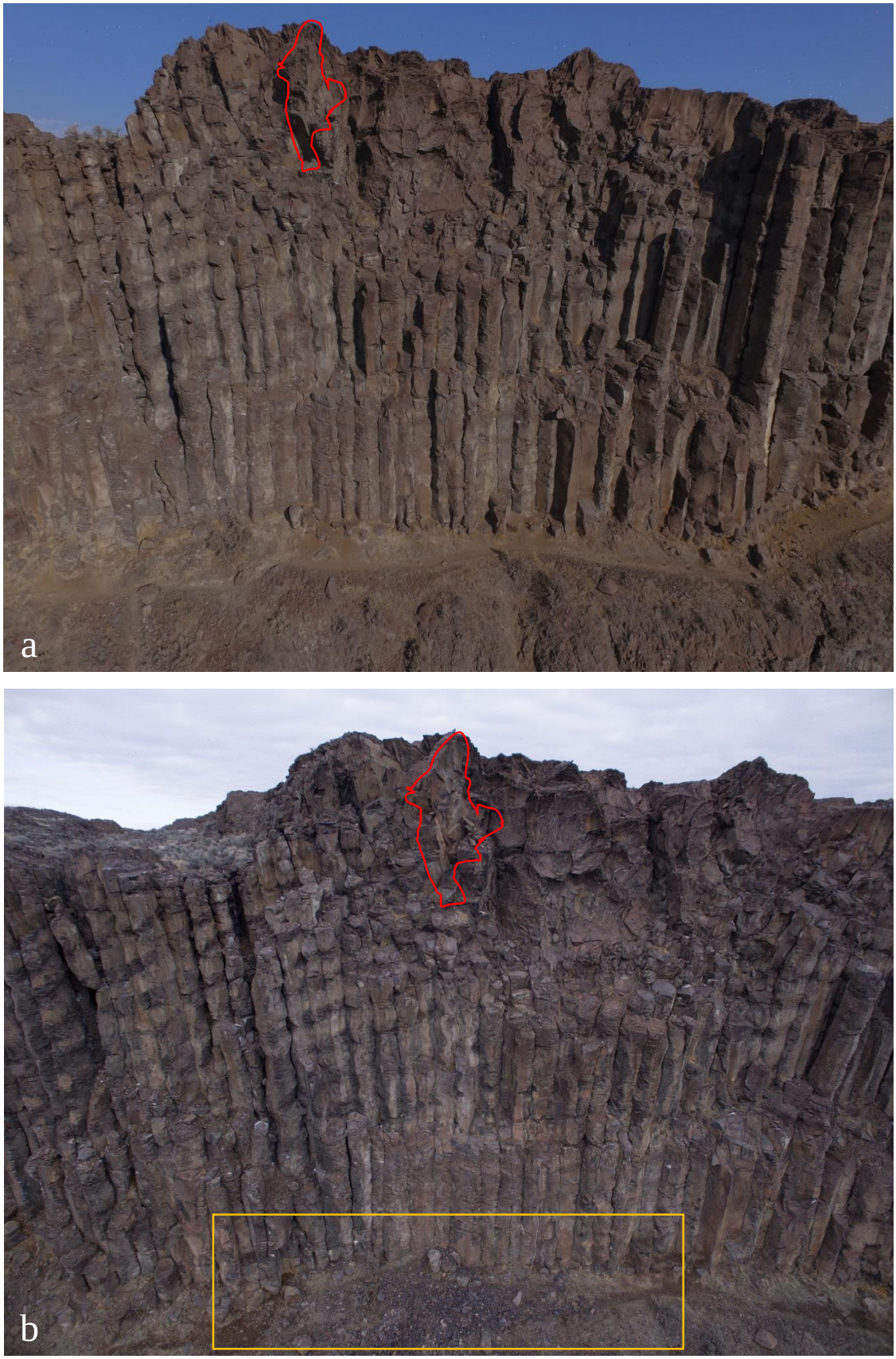

Figure 5: November 2018 Rockfall. These images show a specific section of the Sunshine Wall that was subject to rockfall in late November 2018. At the top of the page the specific block that detached from the rock slope is outlined in red. This picture was taken in October 2018 prior to the event. Below, is an image of the area after the rockfall event. Outlined in Red is the detachment zone. The block that fell was approximately 33 m^3, which is the size of a Volkswagen Beetle. Shown below in yellow is the 33 meter section of trail that was covered in freshly broken talus. The rock is blueish in color due to the freshly fractured-unweathered surfaces.

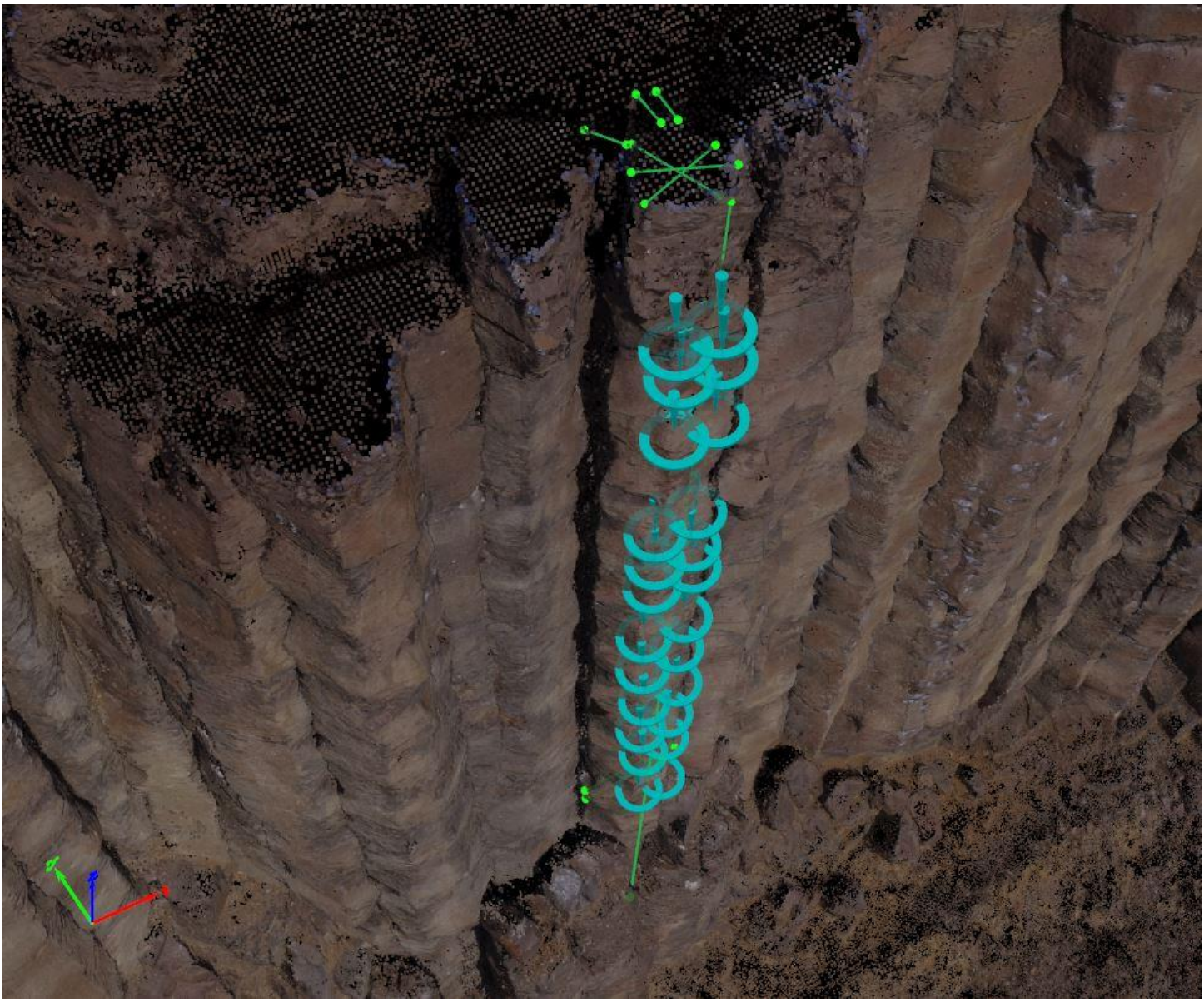

Figure 6: Screen capture of the point cloud in the Pix4D program. The point cloud is much denser across the face of the colonnade than the top, since the majority of photographs were taken at oblique angles to the ground. Green lines demonstrate the ability to take linear measurements within the Pix4D program. Blue pins represent a series of points selected across a particular column face. These points were imported into Matlab for plane fitting which provided accurate dip and dip direction measurements for a number of column faces. The blue, red and green, axes in the lower left corner of the figure represent north, east, and up respectively.

$$\frac{B}{H} > \tan(\Phi) \quad \textit{Stable}$$

$$\frac{B}{H} > \tan(\sin^{-1}(\frac{T}{H}))$$

$$\tan^{-1}(\frac{B}{H}) > \sin^{-1}(\frac{T}{H})$$

$$\sin(\tan^{-1}(\frac{B}{H})) > \frac{T}{H}$$

$$H\left(\frac{B/H}{\sqrt{B^2/H^2+1}}\right) > T$$

$$\left(\frac{B}{\sqrt{B^2/H^2+1}}\right) > T$$

$$\sim B > T \quad \textit{Stable}$$

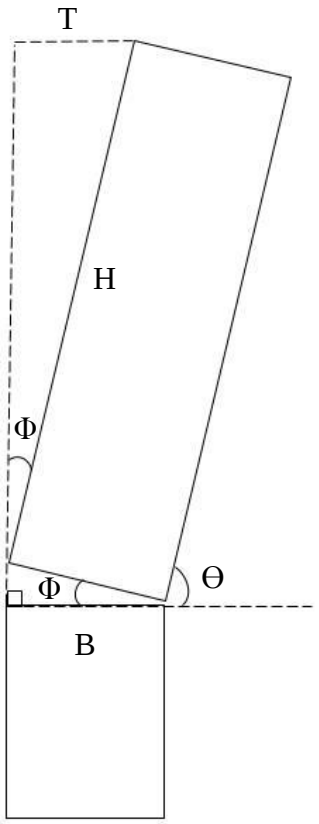

Figure 7: Topple Analysis. This diagram shows the equations and geometry describing center-of-mass problem for individual columns with regard to direct topple failure. B is the diameter of the base of the column; H is the column height; T is the width of the column separation (tension crack) at the top of the slope. Angles theta (Θ) and phi (Φ) are the plunge of the column and the dip of the base, respectively. They are assumed to be complementary (sum to 90°). The final equation assumes that the height of the column is significantly larger than the width, which is the case for the majority of the columns. The sin of inverse tangent was simplified to reach the second to last equation. Since H is generally much larger than B, the first item in the denominator was approximated to equal zero, which is key in arriving to the final equation.

Figure 8: Platy Zone. Adjacent to the notebook is the low RMR zone. This particular column has already failed and only the lower 9 meters of the column remain. The remaining section of this column is supported by the neighboring intact column. The yellow notebook shown is 6 inches across, from left to right.

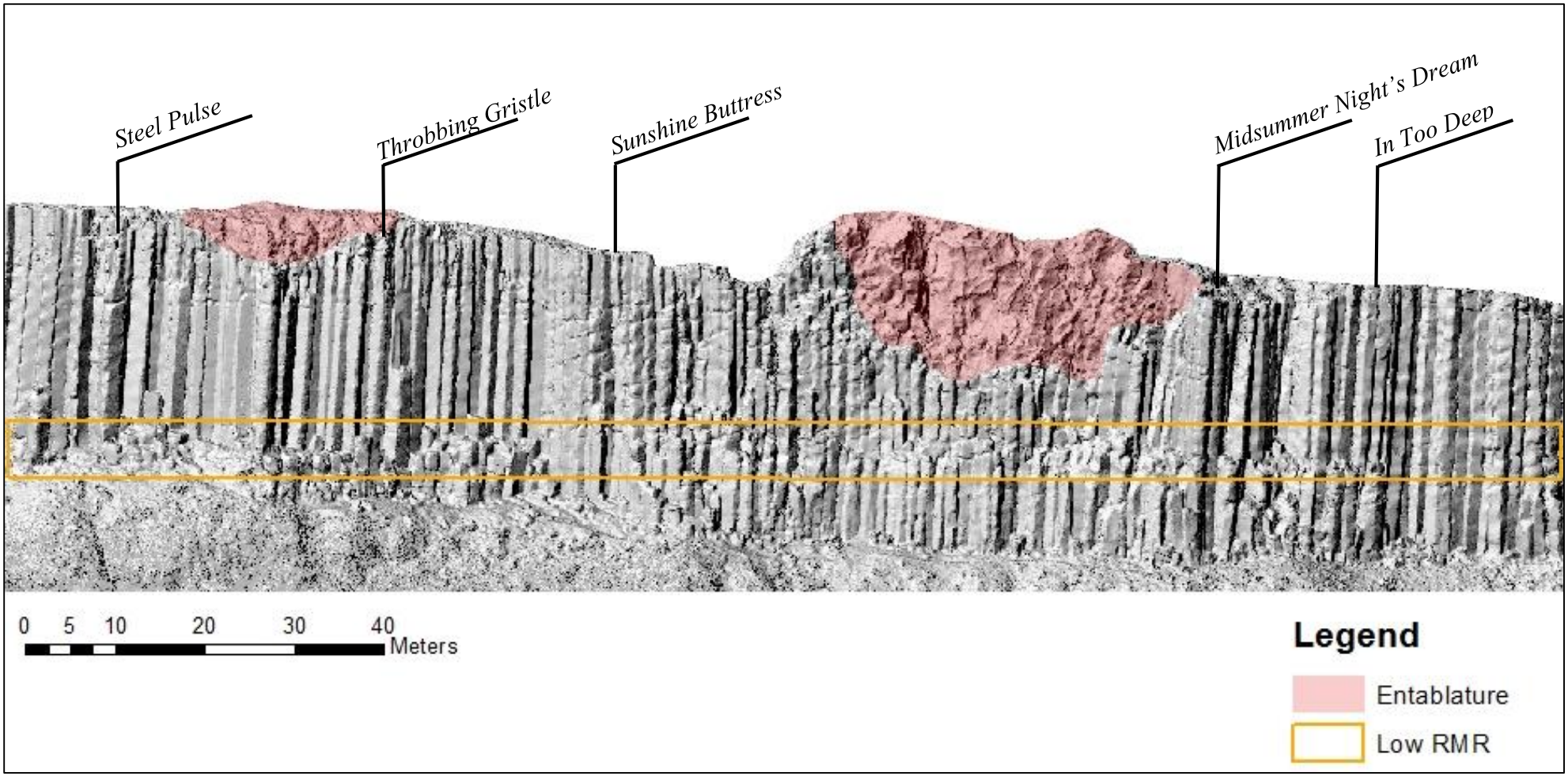

Figure 9: Sunshine Wall DSM. Digital surface model showing the linear feature, outlined in yellow, which crosses the colonnade. Also highlighted, in red, are the zones of entablature which show a different geomorphic texture and style of fracturing. Specific climbing routes have also been labeled. The entablature zone highlighted on the right is where the November 2018 rockfall event took place.

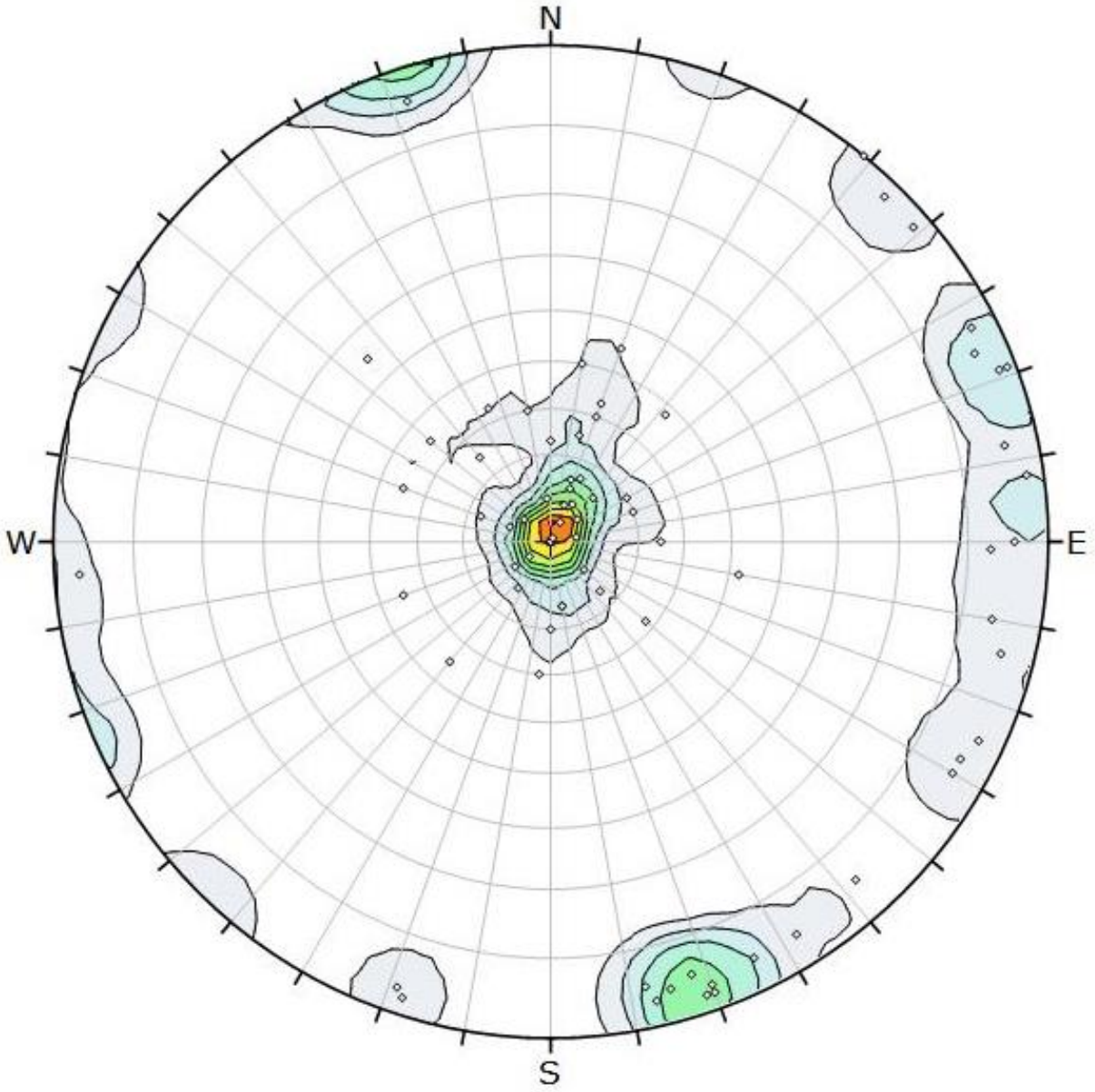

Symbol	Feature
◇	Pole Vectors

Color	Density Concentrations
	0.00 - 2.00
	2.00 - 4.00
	4.00 - 6.00
	6.00 - 8.00
	8.00 - 10.00
	10.00 - 12.00
	12.00 - 14.00
	14.00 - 16.00
	16.00 - 18.00
	18.00 <

Contour Data	Pole Vectors
Maximum Density	18.38%
Contour Distribution	Fisher
Counting Circle Size	1.0%

Plot Mode	Pole Vectors
Vector Count	81 (81 Entries)
Hemisphere	Lower
Projection	Equal Angle

Figure 10: Summary of Discontinuities in the Colonnade. Lower hemisphere projection stereonet displaying discontinuities near the most popular routes across the Sunshine Wall. Points represent poles to joints and fractures measured in the field. Points clustered near the center of the stereonet are representative of through-going discontinuities that cut across the columns. Points along the perimeter represent column-bounding joints.

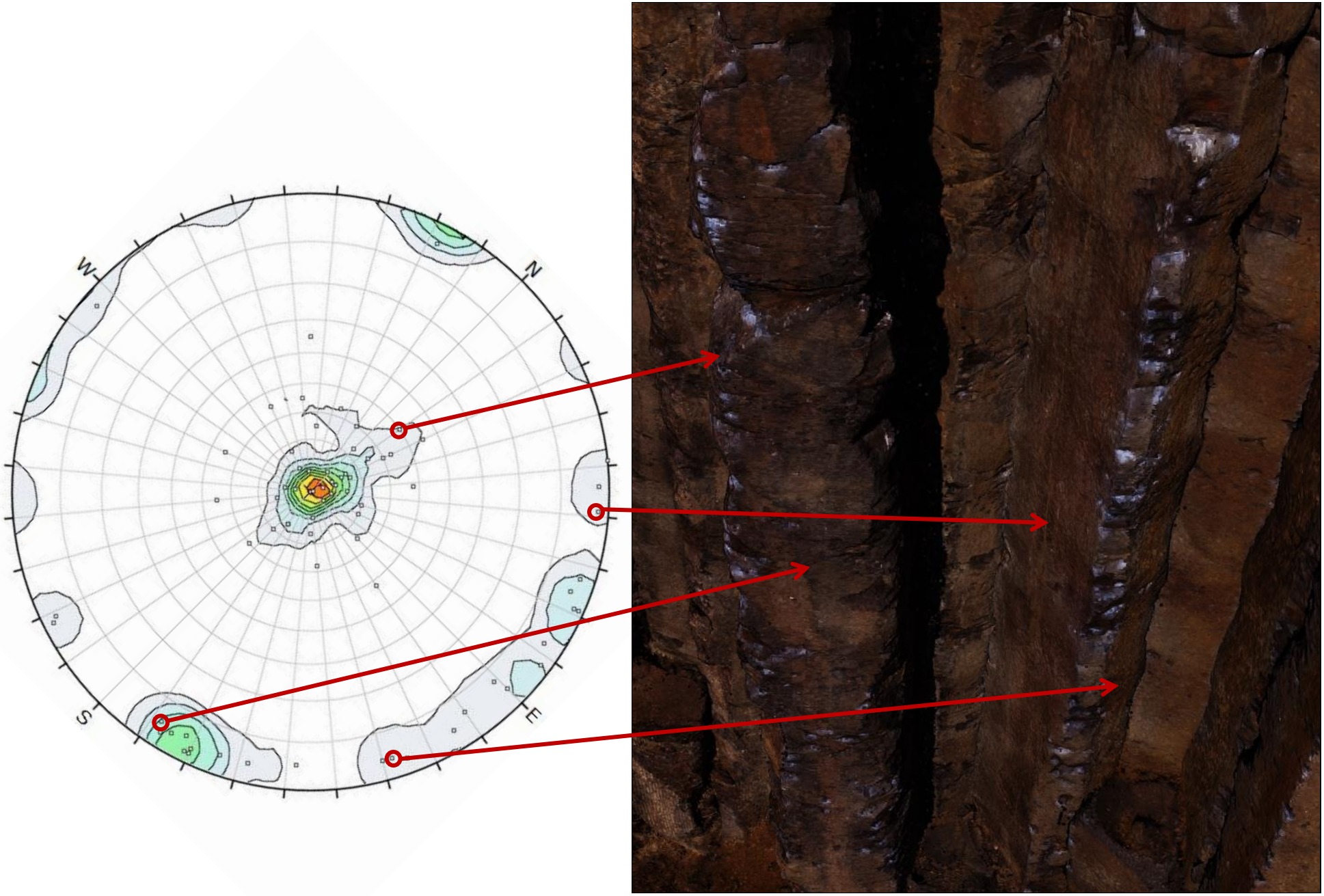

Figure 11. **A**: Mapping of Discontinuities. Specific poles related to the surfaces measured using the 3D digital model. Image at the right is a screen capture from Pix4D showing the climbing routes Steel Pulse on the left, and Narlux on the right.

Figure 11b: This image shows a number of sub-horizontal fractures that are represented by poles plotting in the center of the stereonet. In the upper right corner of the image a set of chains are present, which are used by climbers to descend off the route.

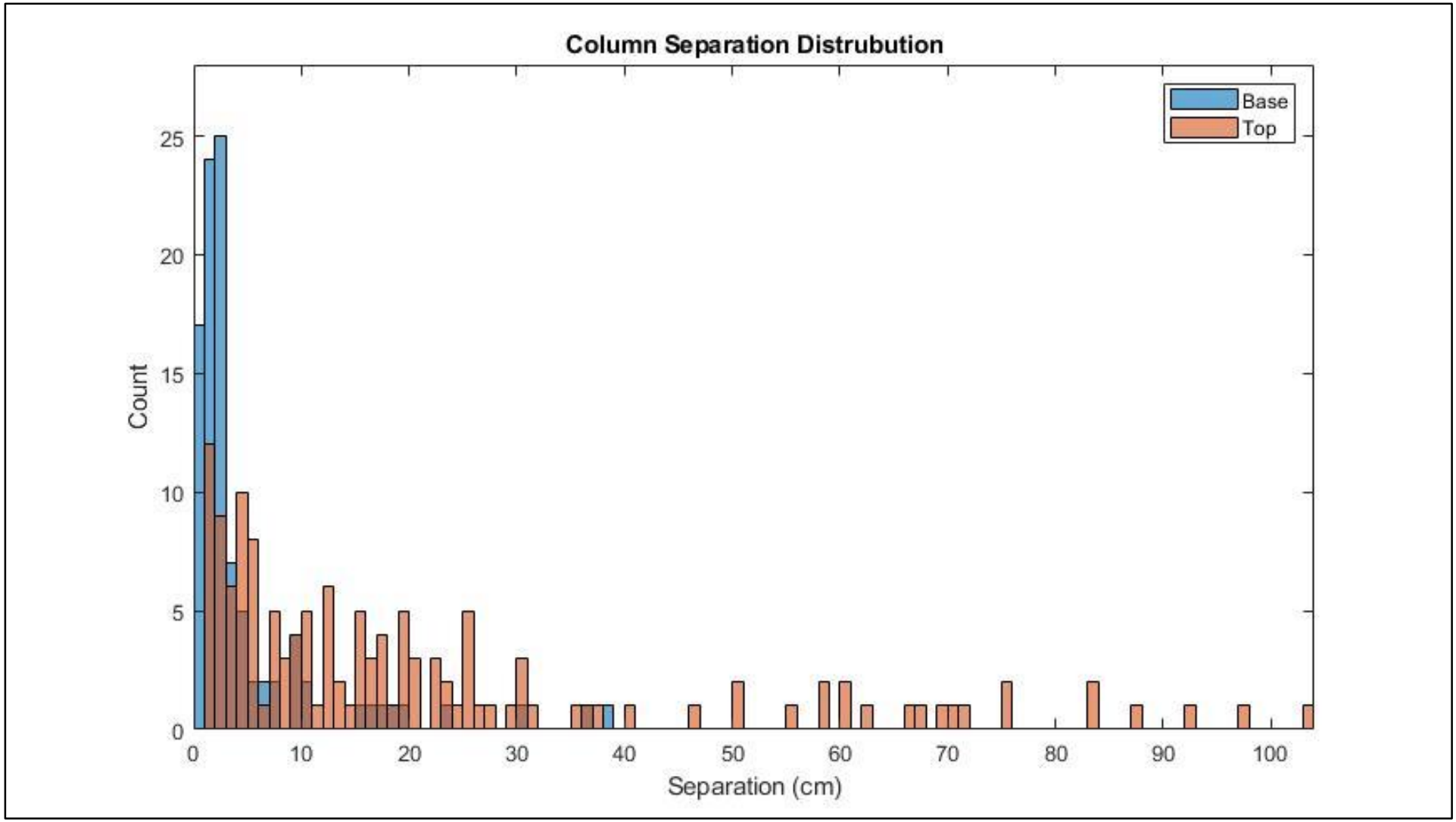

Figure 12: Differential Column Separations. Distribution of column separations at the bottom and top of the colonnade at the Sunshine Wall. Bars that appear darker represent overlapping bar plots.

Figure 13: Column Separations. (a) Vertical aerial photo of the column tops near "Mr. Boshido" with people on the access trail at the foot of the wall. Note that separations appear larger closer to the face of the wall. This area had some of the smallest column separations. Scale bar is relevant to column tops. (b) Large column separation atop the routes Sunshine Buttress and Mix it Up. This separation measures approximately 75 cm.

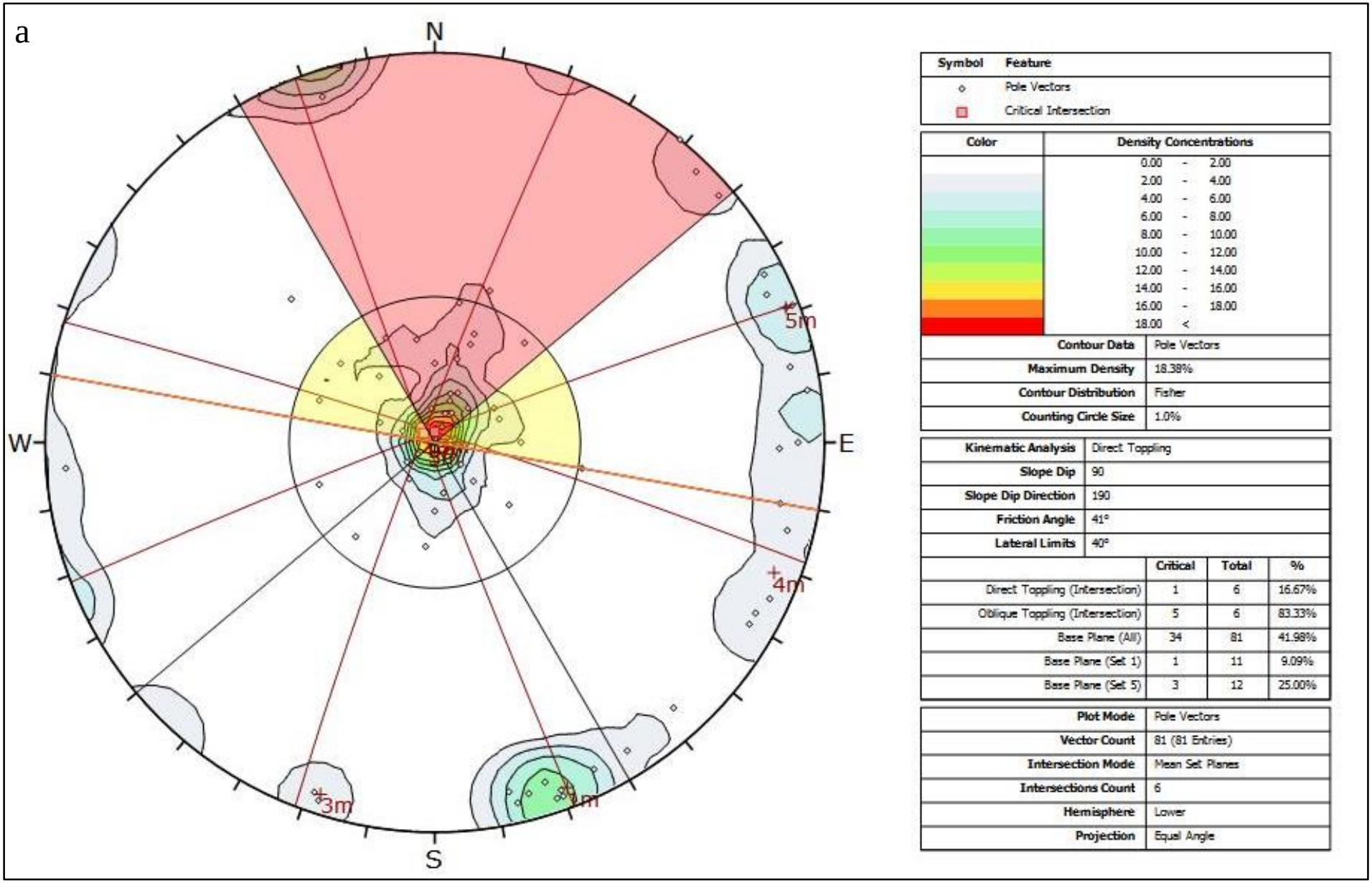

Symbol	Feature
◇	Pole Vectors
▢	Critical Intersection

Color	Density Concentrations
	0.00 - 2.00
	2.00 - 4.00
	4.00 - 6.00
	6.00 - 8.00
	8.00 - 10.00
	10.00 - 12.00
	12.00 - 14.00
	14.00 - 16.00
	16.00 - 18.00
	18.00 <

Contour Data	Pole Vectors
Maximum Density	18.38%
Contour Distribution	Fisher
Counting Circle Size	1.0%

Kinematic Analysis	Direct Toppling
Slope Dip	90
Slope Dip Direction	190
Friction Angle	41°
Lateral Limits	40°

	Critical	Total	%
Direct Toppling (Intersection)	1	6	16.67%
Oblique Toppling (Intersection)	5	6	83.33%
Base Plane (All)	34	81	41.98%
Base Plane (Set 1)	1	11	9.09%
Base Plane (Set 5)	3	12	25.00%

Plot Mode	Pole Vectors
Vector Count	81 (81 Entries)
Intersection Mode	Mean Set Planes
Intersections Count	6
Hemisphere	Lower
Projection	Equal Angle

Figure 14. Kinematic Analysis. Red lines represent mean set planes for column faces. Bolder yellow line is the orientation of Sunshine Wall. Combinations of pole vectors and mean set plane intersections in the red and yellow shaded regions indicate that conditions for the respective failure modes are possible. Each mode has its own specific criteria. (a) Direct Topple analysis, showing the presence of release planes dipping to the south and column faces dipping slightly to the north.

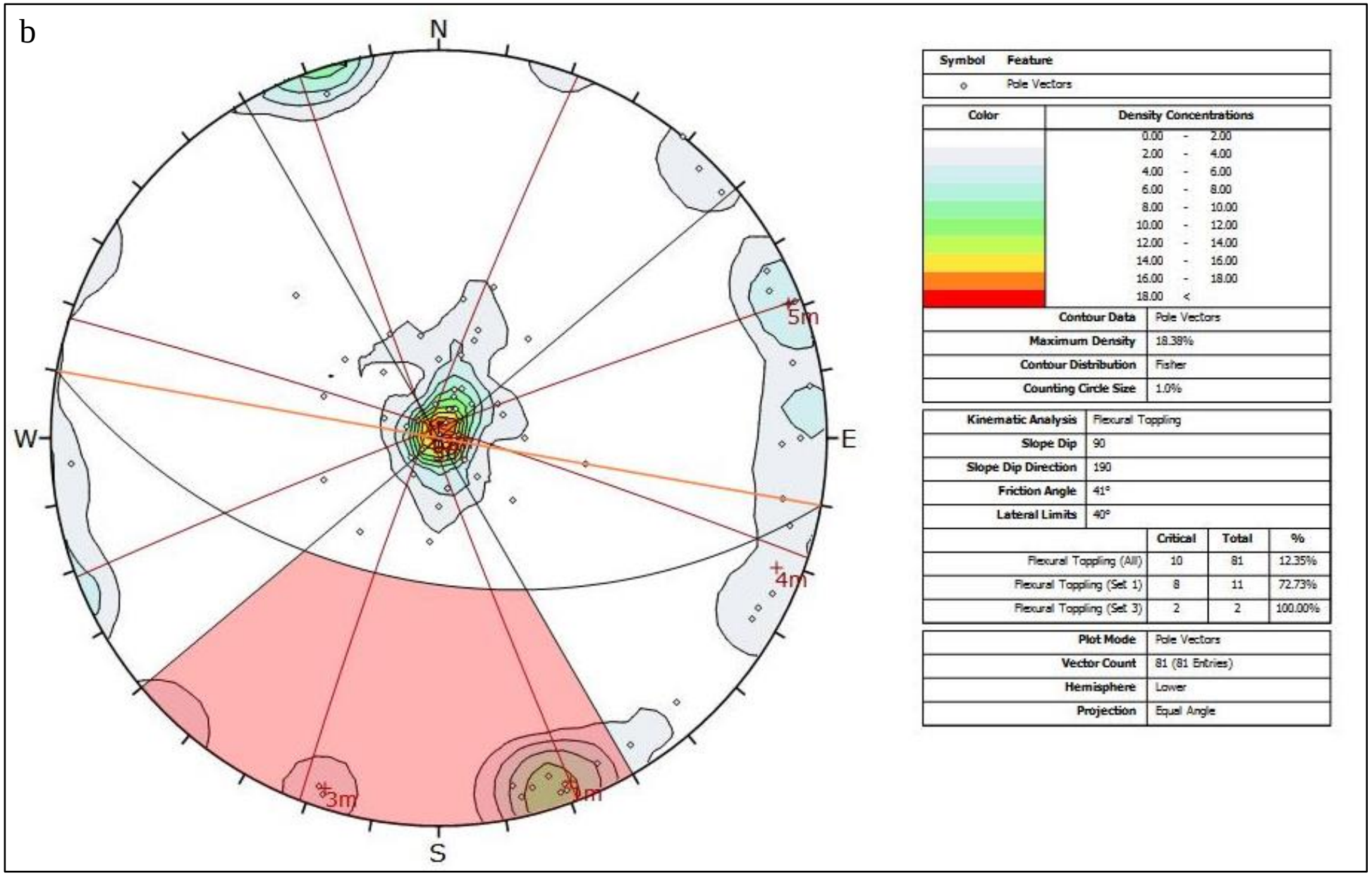

Figure 14 (continued). (b) Flexural Topple, assuming a friction angle of 41° and lateral limits of 40°.

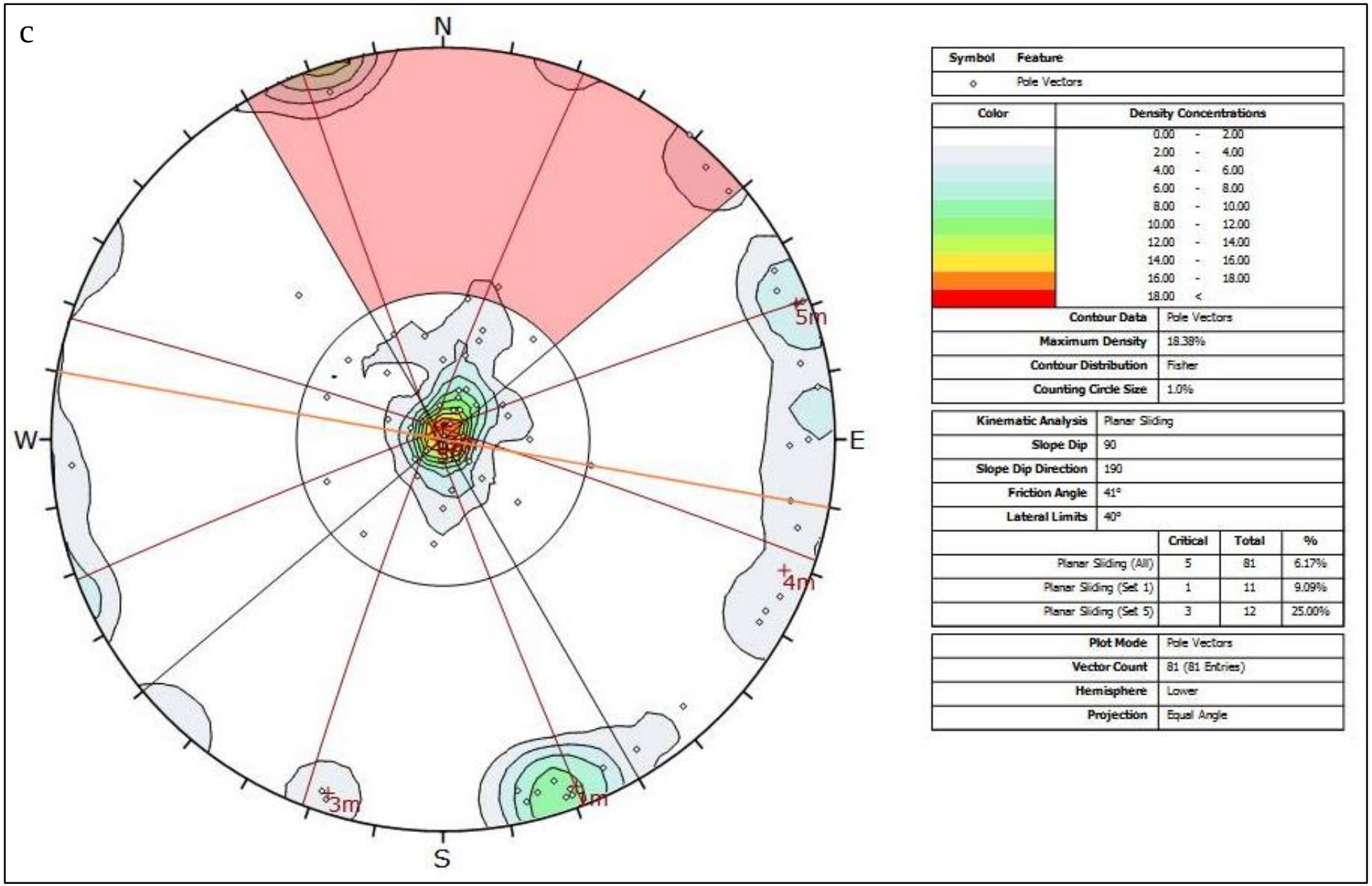

Symbol	Feature
◇	Pole Vectors

Color	Density Concentrations
	0.00 - 2.00
	2.00 - 4.00
	4.00 - 6.00
	6.00 - 8.00
	8.00 - 10.00
	10.00 - 12.00
	12.00 - 14.00
	14.00 - 16.00
	16.00 - 18.00
	18.00 <

Contour Data	Pole Vectors
Maximum Density	18.38%
Contour Distribution	Fisher
Counting Circle Size	1.0%

Kinematic Analysis	Planar Sliding
Slope Dip	90
Slope Dip Direction	190
Friction Angle	41°
Lateral Limits	40°

	Critical	Total	%
Planar Sliding (All)	5	81	6.17%
Planar Sliding (Set 1)	1	11	9.09%
Planar Sliding (Set 5)	3	12	25.00%

Plot Mode	Pole Vectors
Vector Count	81 (81 Entries)
Hemisphere	Lower
Projection	Equal Angle

Figure 14 (continued). Kinematic analysis for sliding failure assuming friction angle of 41° shows few potential slide planes.

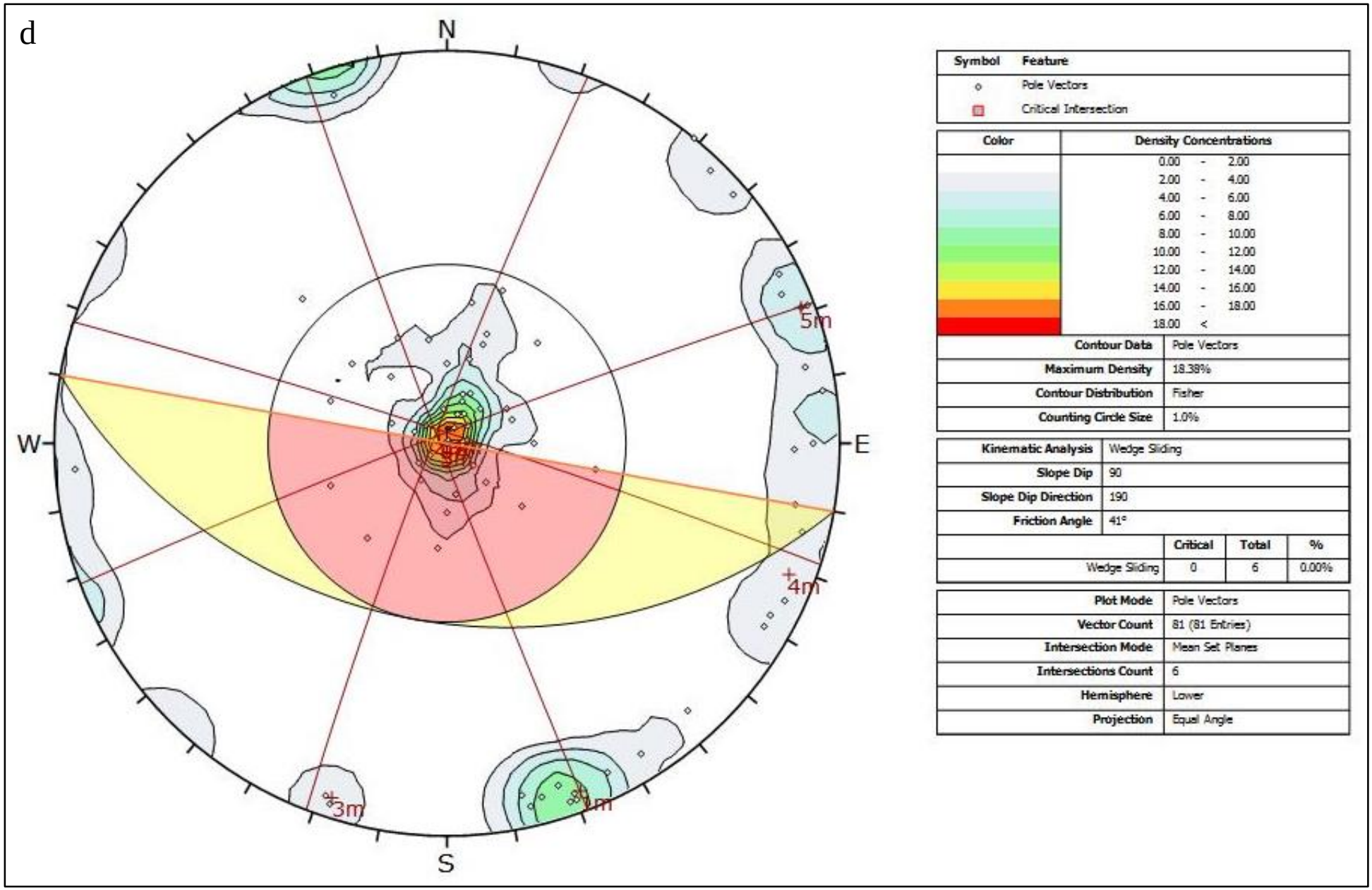

Figure 14 (continued). Kinematic analysis for wedge failure. No intersection lines fall in the red area, indicating wedge failure is not likely.

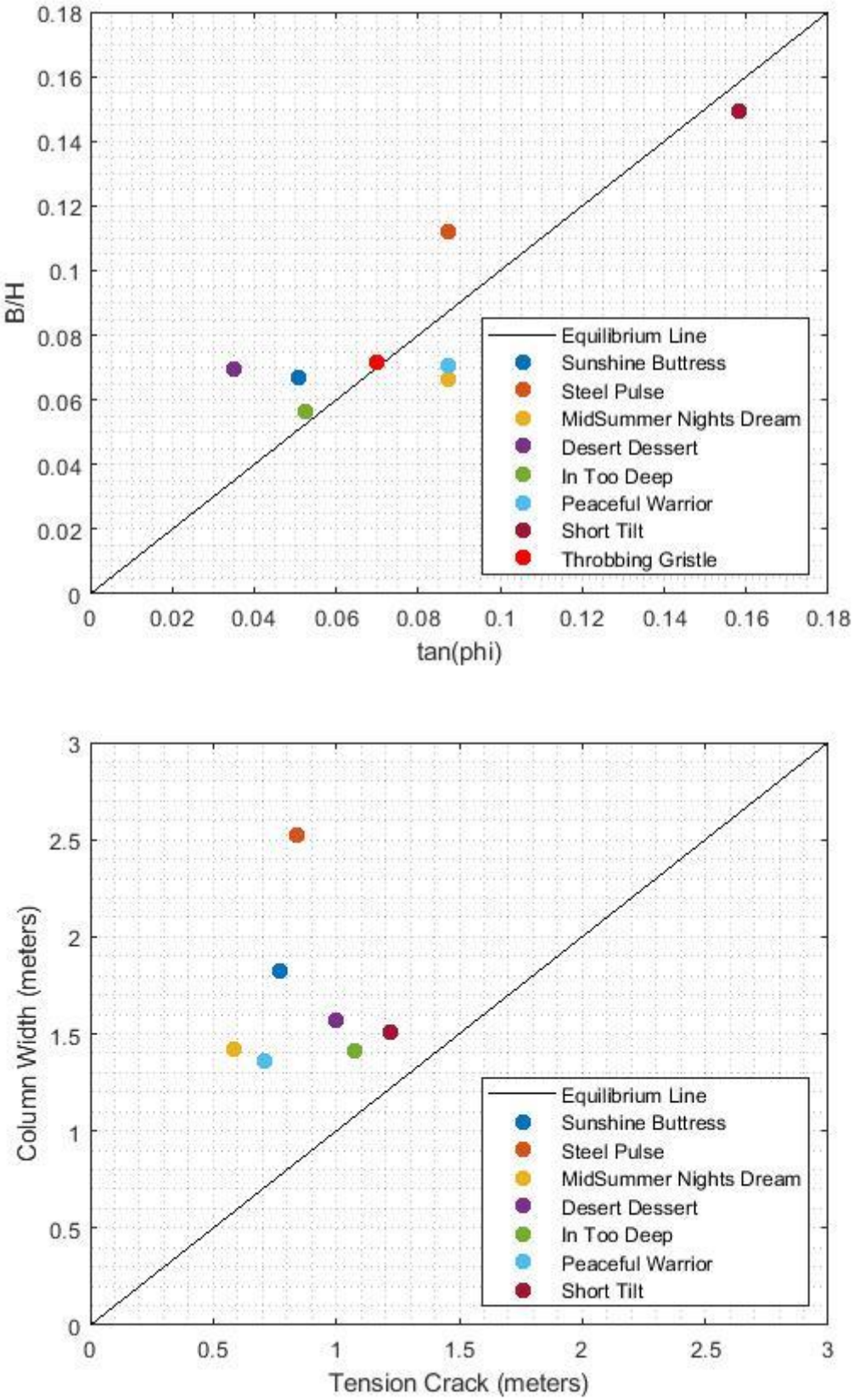

Figure 15. Toppling failure factor-of-safety graphs for specific columns. Points plotting above the equilibrium line have a FS above 1 (considered to be stable). "Throbbing Gristle" is shown in the upper graph only, because the tension crack at the top of the column was not measured during this investigation. Anthropomorphic Chest of Drawers is listed as "Short Tilt".

Figure 16. Image of Midsummer Night's Dream. Red dashed lines show what the column would look like if it were perfectly prismatic. The column is leaning out of the slope (to the right in this picture) and is curves toward that same direction. Column width is 1.4 m. Red bracket at the bottom shows a narrowing base due to weathering and erosion of the column at that location. In the center of this image is a short tilting column, which is the route known as "Anthropomorphic Chest of Drawers".

Figure 17: Image of Anthropomorphic Chest of Drawers. At the base of the exposed portion of the column (indicated in red), the column appears to curve outward. This “kinked” column does not display typical sub-horizontal joints at this location.

Table 1: Summary of column separations**.**

Statistic	**Base separation (cm)**	**Top separation (cm)**
Mean	4.5	24
Median	2	13.5
Mode	2	1
Standard Deviation	7	27
Max	38	111
Min	0.1	1
Count	100	144

Table 2: Differences in Topple Analysis Comparisons. No info is available for Throbbing Gristle because no separation was measured at the top of the column. Asterisks indicate values that were back-calculated from measured parameters. Values are in meters and degrees.

Route Name	T (measured)	T*	dT (meters)	Θ (measured)	Θ*	dΘ (degrees)
Sunshine Buttress	0.77	1.39	0.6	87	88.4	1.3
Steel Pulse	0.84	1.96	1.1	85	87.9	2.9
Midsummer Night's Dream	0.58	1.87	1.3	85.5	88.4	2.9
Desert Dessert	1.0	0.79	0.2	88	87.5	0.5
In Too Deep	1.1	1.31	0.2	87	87.5	0.5
Peaceful Warrior	0.71	1.68	1.0	85	87.9	2.9
Throbbing Gristle	N/A	1.84	N/A	86	N/A	N/A
Short Tilting Column	1.22	1.58	0.4	81	83	2.0

Appendix A (Images of November 2018 rock fall event).

These images were taken from the ground within several days of the rockfall event. In the left picture notice the talus in the foreground and the trail in the background. The picture on the right shows the size of blocks that impacted the trail.

Close up image of detachment zone. The location from which the rock fall originated is outlined in red. Lighter colored surfaces are present showing where fresh fracture surfaces have been exposed. Some loose fractured rock material remains on the cliff face.

Appendix B (Matlab Plane Fitting Scripts)

```
%Ethan Guzek
%Fit 3D Planes to series of points


%% Read in Data

% select te file to be read in
filename=uigetfile('D:\D--Temp\Ethan\*.txt',...
    'Choose one or more CPT data file(s)', 'Multiselect', 'on');
fileID = fopen(filename);
C = textscan(fileID, '%s %f %f %f', 'Delimiter', ',');   %call out like C{1,1} for
string headers in column vector format
fclose(fileID);


name = C{1};
X = C{2}; % easting
Y = C{3}; %northing
Z = C{4}; %elevation

%% Group measurements into categories
compare = strncmp(name(1:end-1), name(2:end), 4);
breaks = find(compare==0);
groups = length(breaks)+1;
planes = {};

while i <= length(groups)
    if(i == 1)
        n = name(1);
        index1 = 1;
        index2 = breaks(1);
    else if(i <= length(breaks))
            n = name(breaks(i));
            index1 = breaks(i-1)+1;
            index2 = breaks(i);
        else if (i > length(breaks))
                n = name(length(X);
                index1 = breaks(i-1)+1;
                index2 = length(X);
            end
        end
    end

    x = X(index1:index2);
    y = Y(index1:index2);
    z = Z(index1:index2);

    [DD, Dip] = Darrel(x,y,z);

    planes{1}(i,1) = n;
    planes{2}(i,1) = DD;
    planes{3}(i,1) = Dip;
end
```

```
%function given vectors x, y, and z

function [DD, Dip] = Darrel(x,y,z)

length = length(x);
a11 = sum(x(1:length).^2);
a12 = sum(x(1:length).*y(1:length));
a13 = sum(x(1:length));
a21 = sum(x(1:length).*y(1:length));
a22 = sum(y(1:length).^2);
a23 = sum(y(1:length));
a31 = sum(x(1:length));
a32 = sum(y(1:length));
a33 = length;

a = [a11 a12 a13;a21 a22 a23; a31 a32 a33];

c1 = sum(x(1:length).*z(1:length));
c2 = sum(y(1:length).*z(1:length));
c3 = sum(z(1:length));

c = [c1;c2;c3];

% This section takes the normal vector to the plane and computes the dip and dip
direction
b = inv(a)*c;
gradient = [-b(1);-b(2);-1];
angle = atand(abs(gradient(1))/abs(gradient(2)));
if(gradient(1) > 0 && gradient(2) > 0)
    dip_direction = 0 + angle;
else if(gradient(1) > 0 && gradient(2) < 0)
        dip_direction = 180 - angle;
    else if(gradient(1) < 0 && gradient(2) < 0)
        dip_direction = 180 + angle;
        else if(gradient(1) < 0 && gradient(2) > 0)
                dip_direction = 360 - angle;
            end
        end
    end
end

dip = asind(sqrt(gradient(1)^2 + gradient(2)^2)/sqrt(gradient(1)^2 + gradient(2)^2 +
gradient(3)^2));

DD = dip_direction;
Dip = dip;
```

Appendix C: Summary of Individual Column Assessments

Sunshine Buttress Area	T	b	h	theta	phi	T*	theta*	phi*	dT	dTheta	b/h	tan(phi)	tan(phi)*
		0.87	1.89	27.16	87.0853	2.9147							
		0.72	1.66	27.33									
		0.87	1.85										
		0.74	1.91										
		0.64											
average:		0.768	1.8275	27.245	87.0853	2.9147	1.385386	88.38469	1.615305	0.617386	1.299395	0.067077	0.050915	0.0282

Steel Pulse	T	b	h	theta	phi	T*	theta*	phi*	dT	dTheta	b/h	tan(phi)	tan(phi)*
		0.87	2.35	22.84	85	5							
		0.81	2.38	22.17									
			2.77										
			2.58										
average:		0.84	2.52	22.505	85	5	1.96144	87.86094	2.139064	1.12144	2.860936	0.111975	0.087489	0.037351

Midsummer Nights Dream	T	b	h	theta	phi	T*	theta*	phi*	dT	dTheta	b/h	tan(phi)	tan(phi)*
		0.52	1.16	17.73	85	5							
		0.68	1.67	18.75	86								
		0.53	1.29	28									
		0.6	1.44										
			1.56										
average:		0.5825	1.424	21.49333	85.5	5	1.873267	88.44701	1.552988	1.290767	2.947012	0.066253	0.087489	0.027111

Desert Dessert	T	b	h	theta	phi	T*	theta*	phi*	dT	dTheta	b/h	tan(phi)	tan(phi)*
		1	1.3	22.86	88	2							
			1.62	22.28									
			1.8										
average:		1	1.573333	22.57	88	2	0.787682	87.46059	2.539413	0.212318	0.539413	0.069709	0.034921	0.04435

In Too Deep	T	b	h	theta	phi	T*	theta*	phi*	dT	dTheta	b/h	tan(phi)	tan(phi)*
		1.11	1.29	25	87	3							
		0.91	1.18										
		1.23	1.23										
		1.06	1.5										
			1.87										
average:		1.0775	1.414	25	87	3	1.308399	87.52979	2.470213	0.230899	0.529787	0.05656	0.052408	0.04314

Peaceful Warrior	T	b	h	theta	phi	T*	theta*	phi*	dT	dTheta	b/h	tan(phi)	tan(phi)*
			1.36	16	85	5							
				22.6									
		0.71											
average:		0.71	1.36	19.3	85	5	1.682106	87.89175	2.108248	0.972106	2.891752	0.070466	0.087489	0.036812

Throbbing Gristle	T	b	h	theta	phi	T*	theta*	phi*	dT	dTheta	b/h	tan(phi)	tan(phi)*
	NA		1.84	26.33	86	4							
			1.94										
			1.85										
average:	NA		1.876667	26.33	86	4	1.836688	NA	NA	NA	NA	0.071275	0.069927	NA

Short Tilting Column	T	b	h	theta	phi	T*	theta*	phi*	dT	dTheta	b/h	tan(phi)	tan(phi)*
		1.22	1.48	10.11	81	9							
			1.48										
			1.57										
average:		1.22	1.51	10.11	81	9	1.581552	83.06908	6.930922	0.361552	2.069078	0.149357	0.158384	0.121561

Appendix D: Discontinuity and Tilt Test Data

Dip	Dip Direction
0	0
15	198
0	0
5	206
13	200
8	230
6	260
10	175
16	205
16	315
9	200
25	140
20	250
8	130
13	35
14	224
33	155
42	280
0	0
0	0
0	0
35	70
25	270
20	240
25	195
0	0
35	110
10	110
20	0
15	350
30	200
45	200
33	200
30	5
10	55
55	135
15	350
28	310
10	310
0	130
35	130
17	110

0	0
30	170
40	190
6	55
1	210
10	210
35	40
23	180
38	222
85	342
88	262
84	280
86	328
86	258
87	19
83	271
86	246
88	341
86	162
87	86
86	270
86	345
90	219
87	295
87	243
87	340
86	300
88	224
86	284
88	340
88	229
86	298
85	348
88	249
86	334
88	18
89	249
85	318
87	347

Tilt Tests:

Data

Combination Number	Test #1 (Degrees)	Test #2 (Degrees)
1	44	41
2	41	40
3	39	34
4	41	44
5	41	45
6	43	44
7	36	41
8	40	40
9	39	42
10	41	43

Mean	41
Median	41
Mode	41
Standard Deviation	2.68
Max	45
Min	34
Average Differential	2.7